Impact of nitrous acid photolysis on the total hydroxyl radical budget during the Limitation of Oxidant Production/Pianura Padana Produzione di Ozono study in Milan

B. Alicke[1] and U. Platt
Institut für Umweltphysik, Heidelberg, Germany

J. Stutz
Department of Atmospheric Sciences, University of California, Los Angeles, California, USA

Received 19 October 2000; revised 12 July 2001; accepted 12 July 2001; published 7 November 2002.

[1] The photolysis of nitrous acid (HONO) in the early morning hours is believed to be a significant source of hydroxyl radicals (OH), the most important daytime oxidizing species. Although the importance of this mechanism has been recognized for many years, no accurate experimental quantification is available. Here we present measurements of HONO, NO_2, SO_2, O_3 and HCHO by Differential Optical Absorption Spectroscopy (DOAS) during the Limitation of Oxidant Production/Pianura Padana Produzione di Ozono (LOOP/PIPAPO) study in May–June 1998 in Milan, Italy. The concentration of NO and $J(NO_2)/J(HONO)$ were simultaneously monitored by in situ monitors. The photolysis frequencies of HCHO and O_3 were determined with a radiative transfer model. High nocturnal HONO mixing ratios of up to 4.4 ppb were regularly observed. Elevated daytime HONO levels during cloudy periods show that the formation of HONO proceeds after sunrise and therefore also represents a source of hydroxyl radicals throughout the day. Averaged over 24 hours, HCHO photolysis is the most important source of OH in Milan, followed by either ozone or HONO photolysis. Our observations indicate that on certain days the OH production from HONO can be even more important than that from ozone photolysis. The diurnal variation of the different OH formation mechanisms shows that HONO photolysis is by far the most important source in the early hours of the morning, and can be as large as and even surpass the total OH production at noon. *INDEX TERMS:* 0365 Atmospheric Composition and Structure: Troposphere—composition and chemistry; 0345 Atmospheric Composition and Structure: Pollution—urban and regional (0305); 0394 Atmospheric Composition and Structure: Instruments and techniques; *KEYWORDS:* nitrous acid, HONO, nocturnal chemistry, hydroxyl radical, OH radical

Citation: Alicke, B., U. Platt, and J. Stutz, Impact of nitrous acid photolysis on the total hydroxyl radical budget during the Limitation of Oxidant Production/Pianura Padana Produzione di Ozono study in Milan, *J. Geophys. Res.*, *107*(D22), 8196, doi:10.1029/2000JD000075, 2002.

1. Introduction

[2] The photolysis of nitrous acid (HONO) has long been recognized as a potentially important production mechanism for OH radicals in the polluted urban atmosphere [*Calvert et al.*, 1994; *Harris et al.*, 1982; *Jenkin et al.*, 1988; *Kessler et al.*, 1981; *Lammel and Cape*, 1996; *Perner and Platt*, 1979; *Platt*, 1986; *Platt and Heintz*, 1994; *Platt et al.*, 1980]. Upon irradiation with UV light HONO decomposes, forming an OH radical and NO [*Stockwell and Calvert*, 1978; *Stutz et al.*, 2000]:

$$\mathrm{HONO} + h\nu \rightarrow \mathrm{OH} + \mathrm{NO} \quad (300\ \mathrm{nm} < \lambda < 405\ \mathrm{nm}). \qquad (1)$$

[3] The OH radical is the central compound in the formation of ozone in the troposphere (see, for example, the review by *Crutzen and Zimmermann* [1991]), and the quantification of OH formation mechanisms is essential for the understanding of tropospheric chemistry. Peak daytime hydroxyl radical concentrations in the range $(2–10) \times 10^6$ cm^{-3} have been measured at the surface in the midlatitudes during summer [*Brauers et al.*, 1996; *Eisele et al.*, 1997; *Holland et al.*, 1995, 1998]. A diurnally and annually averaged global mean tropospheric OH concentration has been estimated to be $0.7–1.0 \times 10^6$ cm^{-3} [*Crutzen and Zimmermann*, 1991; *Prinn et al.*, 1995].

[1] Also at Department of Atmospheric Sciences, University of California, Los Angeles, California, USA.

0148-0227/02/2000JD000075$09.00

[4] A number of other mechanisms form OH radicals:

1. The reaction of $O(^1D)$ atoms, formed in the photolysis of O_3 at wavelengths below 320 nm, with water (reactions (2)–(3)) [*Crutzen and Zimmermann*, 1991; *Levy*, 1973; *Logan et al.*, 1981] is the most important mechanism on a global scale.

$$O_3 + h\nu \rightarrow O(^1D) + O_2 \quad (\lambda < 320\ \text{nm}), \tag{2}$$

$$O(^1D) + H_2O \rightarrow 2\ OH, \tag{3}$$

$$O(^1D) + M \rightarrow O(^3P) + M \qquad M = (N_2 \text{ or } O_2). \tag{4}$$

2. The photolysis of aldehydes can form RO_2 radicals, which are converted to OH radicals in the presence of NO. Reactions (5)–(9) show this mechanisms for the most abundant aldehyde, formaldehyde [e.g., *Crutzen and Zimmermann*, 1991; *Ehhalt et al.*, 1998; *Fried et al.*, 1997; *Kleinman et al.*, 1995; *Meller and Moortgart*, 2000].

$$HCHO + h\nu(\lambda < 370\ \text{nm}) \rightarrow H + HCO, \tag{5}$$

$$HCHO + h\nu(\lambda < 370\ \text{nm}) \rightarrow H_2 + CO, \tag{6}$$

$$H + O_2 \rightarrow HO_2 \tag{7}$$

$$HCO + O_2 \rightarrow HO_2 + CO \tag{8}$$

$$HO_2 + NO \rightarrow OH + NO_2 \tag{9}$$

Typical mixing ratios of formaldehyde in polluted areas are of the order of 10 ppb, and photolysis frequencies for reaction (5) at noon are around $3 \times 10^{-5}\ s^{-1}$ for clear skies. Formaldehyde is also formed by the oxidation of hydrocarbons and can therefore be considered to be, at least partially, a secondary source of OH. The mixing ratios of some higher aldehydes can reach levels similar to those of HCHO, but their photolysis frequencies are about an order of magnitude smaller. Nevertheless, the sum of OH formation from larger aldehydes can be important [*Finlayson-Pitts and Pitts*, 2000].

3. The reaction of ozone with alkenes can lead to the direct production of OH radicals with yields from 7 to 100% [*Atkinson and Aschmann*, 1993; *Atkinson et al.*, 1992; *Paulson et al.*, 1997; *Donahue et al.*, 1998; *Finlayson-Pitts and Pitts*, 2000; *Paulson et al.*, 1999]).

4. The reaction of RO_2 with NO can represent another net source of OH radicals. Sources of RO_2 that contribute to formation of OH radicals can be the ozonolysis of alkenes, nighttime reactions of NO_3 with alkenes [*Carslaw et al.*, 1997; *Geyer et al.*, 2002; *Mihelcic et al.*, 1993; *Platt et al.*, 1990], and OH hydrocarbon reactions that yield more than one RO_2 radical.

[5] The relative importance of the individual OH formation mechanisms depends on the actinic flux and the degree of pollution. Owing to its lower dissociation energy threshold, the photolysis of HONO accumulated during the night is the first mechanism forming OH in the morning, followed by the photolysis of HCHO. The photolysis of O_3 requires actinic fluxes in the lower UV and becomes important only later in the day. In contrast, the reaction of ozone with alkenes does not require sunlight and also proceeds during the night. Concentrations of HONO and HCHO typically increase with the degree of pollution, and these sources then become more significant. In very polluted situations, large nighttime NO emissions near the ground often titrate ozone making ozone photolysis and ozone + alkene reactions less important in the late night and early morning. Nighttime OH formation mechanisms involving ozone are therefore inefficient and become efficient only after the breakup of the nocturnal inversion and the dilution of the NO by entrainment from ozone aloft.

[6] Since its first identification by *Perner and Platt* [1979] and *Platt and Perner* [1980] many atmospheric measurements of HONO have been reported (see *Calvert et al.* [1994] or *Lammel and Cape* [1996] for recent reviews). Photolysis, NO_2 levels, and vertical mixing [*Febo et al.*, 1996] dominate the diurnal variation of the HONO mixing ratio. HONO concentrations typically increase during the night, showing a maximum before sunrise. The fast photolysis during sunrise is followed by a period of low concentrations during the day.

[7] Several studies have discussed the importance of HONO photolysis as an OH source based on different assumptions about the formation of HONO. OH production rates were estimated in the range of $(0.1–3) \times 10^7$ molecules $cm^{-3}s^{-1}$ [*Harris et al.*, 1982; *Sjödin*, 1988] for up to 8 ppb of nitrous acid (measurements in Los Angeles) in the morning hours. Calculations by *Harris et al.* [1982] show an increase of the maximum ozone concentration of up to 55% during the course of the day if 4% of the initial NO_x is present as HONO (Los Angeles case, initial NO_x: 0.24 ppm). *Jenkin et al.* [1988] showed in a model study that photolysis of HONO in the early morning could account for a fivefold increase in OH at 0600, a 14% increase in OH present at the daily maximum (noon), and a 16% increase in net photochemical ozone production. They also showed that the increase of ozone starts much earlier owing to the HONO photolysis in the morning. *Staffelbach et al.* [1997a, 1997b] investigated the influence of HONO in the plume of Milan. Assuming a direct emission of HONO of 10% of the emitted NO_x, they calculated only small changes in OH and ozone concentrations in the lowest layer of the atmosphere.

[8] In order to assess the importance of HONO as a precursor of the OH radical, its sources and sinks must be well known. The only important gas phase reaction forming nitrous acid is [*Nguyen et al.*, 1998; *Pagsberg et al.*, 1997; *Stuhl and Niki*, 1972; *Zabarnick*, 1993]

$$OH + NO(+\ M) \rightarrow HONO(+\ M). \tag{10}$$

[9] Since this reaction removes OH, subsequent photolysis does not represent a net source of OH radicals. The bulk of urban HONO is suspected to be formed from either of the mechanisms summarized in reactions (11) or (12), involving only NO_x and water [*Kessler and Platt*, 1984; *Perner and Platt*, 1979; *Platt*, 1986]:

$$NO_2 + NO + H_2O \rightarrow 2\ HONO, \tag{11}$$

$$2\ NO_2 + H_2O \rightarrow HONO + HNO_3. \tag{12}$$

These reactions seem to proceed heterogeneously on surfaces [*Ammann et al.*, 1998; *Calvert et al.*, 1994;

Goodman et al., 1999; *Junkermann and Ibusuki*, 1992; *Kalberer et al.*, 1999; *Lammel and Perner*, 1988; *Longfellow et al.*, 1998; *Notholt et al.*, 1991, 1992; *Sakamaki et al.*, 1983]. A number of laboratory studies [*Jenkin et al.*, 1988; *Kleffmann et al.*, 1998; *Pitts et al.*, 1984b; *Sakamaki et al.*, 1983; *Svensson et al.*, 1987] and field studies [*Harrison and Kitto*, 1994; *Kessler and Platt*, 1984] have suggested that reaction (11) is not significant.

[10] The exact mechanism of the heterogeneous formation of HONO summarized in reaction (12) is unknown, but several studies [*Jenkin et al.*, 1988; *Kleffmann et al.*, 1998; *Svensson et al.*, 1987] have shown that it is first order in NO_2 and water. Neither the reaction rate constants nor the nature of the surface is known, which makes calculation of the OH production by models difficult.

[11] Several studies have been carried out to estimate the strength of direct emission of nitrous acid from combustion processes [*Ackermann*, 2000; *Kessler and Platt*, 1984; *Kirchstetter et al.*, 1996; *Pitts et al.*, 1984a; *Winer and Biermann*, 1994]. Up to 1% of the emitted NO_x was found as nitrous acid, making this source important, especially in heavily polluted areas with high amounts of traffic. *Kirchstetter et al.* [1996] report a $HONO/NO_x$ emission ratio of 0.35% for a North American car fleet, while *Ackermann* [2000], found a value of 0.65% in a traffic tunnel in Germany.

[12] A number of chemical removal processes for HONO, besides photoloysis, are known. A few percent of HONO is expected to be destroyed by OH radicals:

$$OH + HONO \rightarrow H_2O + NO_2. \quad (13)$$

The self-reaction of HONO in reaction (14) [*Chan et al.*, 1976] and the reaction of HONO with nitric acid in reaction (15) [*Kaiser and Wu*, 1977] in the gas phase are too slow to be important, but an acceleration of these reactions on surfaces has been reported [*Svensson et al.*, 1987]:

$$2\ HONO \rightarrow NO + NO_2 + H_2O, \quad (14)$$

$$HONO + HNO_3 \rightarrow 2\ NO_2 + H_2O. \quad (15)$$

[13] Although the photolysis of HONO is a potentially important source of OH radicals, an accurate quantification of the OH production through this process in the atmosphere is missing in the literature. The quantification of the OH production is difficult because it requires the fast and precise measurement of HONO during sunrise. Most published measurements were performed with instruments of 0.5–12 hour time resolution [*Appel et al.*, 1990; *Febo et al.*, 1993; *Harrison et al.*, 1996; *Sjödin and Ferm*, 1985], too slow to follow the decrease of HONO at sunrise. The recent improvement of differential optical absorption instruments (DOAS) in our laboratory has increased the time resolution to typically 3–5 min, fast enough to follow HONO photolysis and to determine the OH production at sunrise.

[14] Here we present measurements of HONO, its precursor NO_2, HCHO, and O_3 by DOAS during the Limitation of Oxidant Production/Pianura Padana Produzione di Ozono (LOOP/PIPAPO) field campaign 1998. The NO_2 and HONO photolysis frequencies were also measured. A radiative transfer model was employed to calculate J(HCHO) and $J(O_3 \rightarrow O(^1D))$. The measurements are used to calculate the OH production rates of the different mechanisms and to determine the relative importance of HONO photolysis.

2. Experimental Methods

2.1. Measurement Site

[15] The measurements were performed during the Limitation of Oxidant Production/Pianura Padana Produzione di Ozono (LOOP/PIPAPO) campaign in Milan, Italy (45°32′N, 9°12′E). The instruments were set up in a heavy trailer on a military helicopter base in Bresso, 8 km north of the city center. The site is a flat area of 2 × 4 km surrounded by a combination of a residential area with some light industry. The highway A4, which connects Novarra to Bergamo, runs ~500 m north of the airfield (see Figure 1). The civil airport in the west and the military base had little air traffic during the day and none at night.

[16] The trailer housed a DOAS telescope, which was mounted 1.8 m above the ground and aimed at three retroreflector arrays (each seven quartz cube corner prisms) located at three different heights (0.9–1.5, 2.45, and 4 m above ground) 1.25 km to the north. The different heights were scanned consecutively. These gradient measurements will be presented by *Stutz et al*, [2002] Here we focus primarily on the results from the highest light path. The time resolution for taking a complete spectrum at one height was around 5–15 min. Commercial systems were used to determine the NO concentration (chemiluminescence detector, CLD 770 ppt by Eco Physics) and the photolysis frequency of NO_2 (filter radiometer, Meteorology Consult, 4π sr $J(NO_2)$ Radiometer 631/632). A sonic anemometer (Gill 4K) was set up 250 m north of the trailer at 2.2 m height, and provided micrometeorological data. Volatile Organic Compounds (VOC) were measured at the civil airport by *Grüebler* [1999] with a gas chromatograph (Airmo VOC HC1010). Measurement procedures and data evaluation techniques are described by *Grüebler* [1999].

2.2. The DOAS Instrument

[17] Differential optical absorption spectroscopy (DOAS) is a technique that identifies and quantifies trace gases with narrowband absorption structures in the near UV and visible wavelength region in the open atmosphere (see, for example, the review by *Platt* [1994]). The fundamental setup of a DOAS system consists of a broadband light source, an optical setup that transfers the light through the atmosphere, and a spectrograph-detector system to record the absorption spectra. Because broadband extinction by Mie scattering and turbulence are unknown, these interferences have to be corrected to derive trace gas concentrations. The basic idea of DOAS is therefore to separate the trace gas absorption cross section into two parts, one that varies slowly with wavelength, and a fast varying differential cross section σ'. If the same filtering procedure is applied to the atmospheric absorption spectrum, the narrowband absorption can be used to calculate the trace gas concentrations [*Platt*, 1994]. The advantages of DOAS are the unequivocal and absolute identification of the trace gases and the fact that trace gas concentrations are determined solely on the basis of the absorption cross section. A calibration is therefore not necessary.

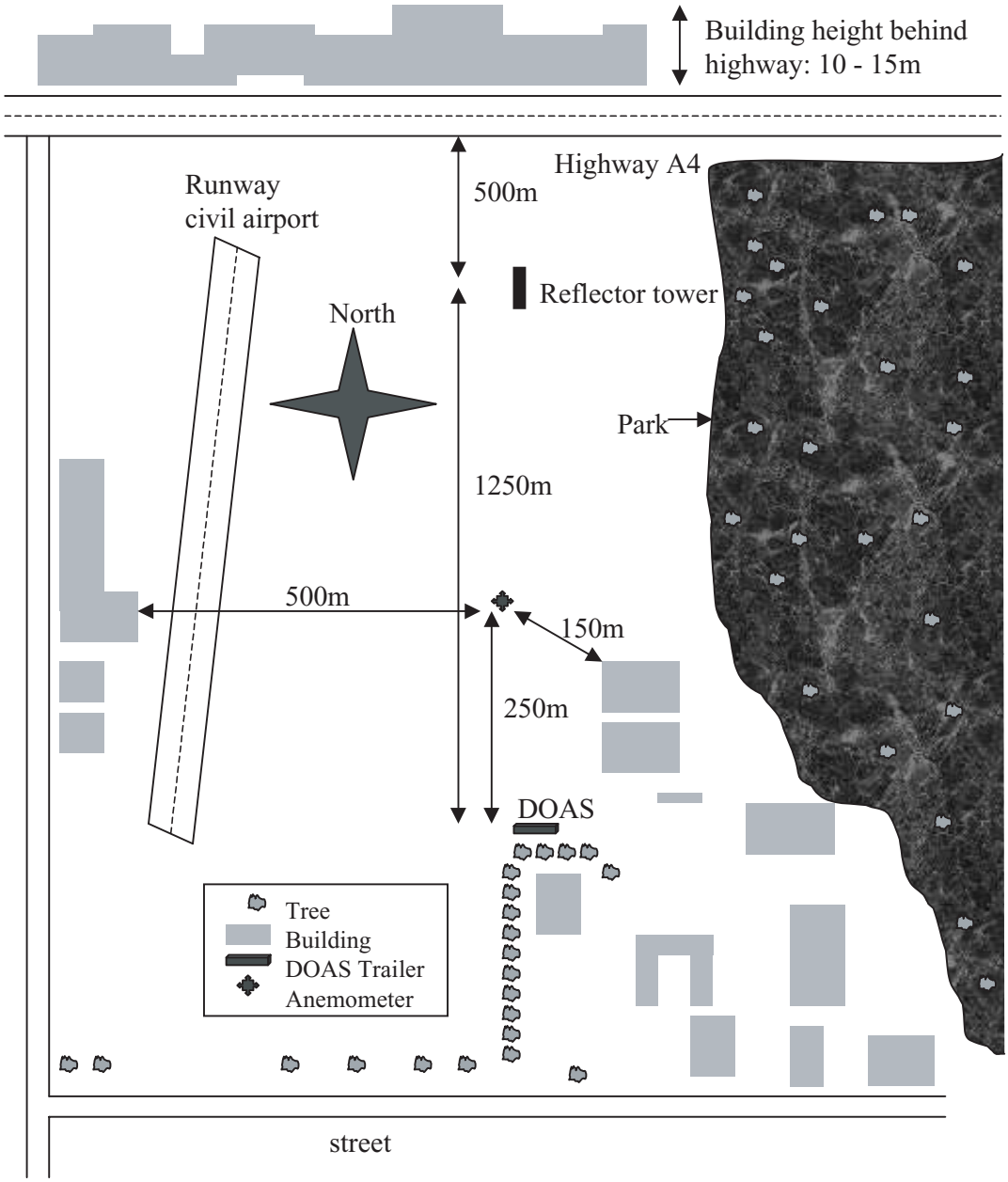

Figure 1. Setup of the system and the reflector tower at the military base in Bresso, Italy. The in situ measurement systems were set up in the trailer together with the long-path differential optical absorption spectroscopy (LP-DOAS) telescope. The sonic anemometer was located close to the light path about 250 m north of the trailer.

[18] A new design of a long-path DOAS system [*Stutz*, 1996], based on the principle of *Platt and Perner* [1980], was used in Milan. It incorporates two coaxially arranged Newtonian telescopes that collimate, send, and receive the light beam of a Xe short-arc lamp. The light path is folded once by a retroreflector array mounted at a distance of 1.25 km. The spectrograph was coupled to the telescope by a quartz fiber, which also performed the task of a mode mixer as described by *Stutz and Platt* [1997]. Spectra in the UV were recorded at a resolution of about 0.55 nm by a Czerny-Turner spectrograph with a focal length of 0.5 m ($F = 6.9$, 600 groves mm^{-1} grating, thermostated to $+25° \pm 0.3°C$). A photodiode array detector [*Stutz and Platt*, 1992] (Hoffmann Meßtechnik, using an array from Hamamatsu S5931-1024N; 1024 diodes of 25 μm center to center spacing, height: 2.5 mm) was used for the detection of the spectra. The array was cooled by a Peltier element to $-15° \pm 0.3°C$ to reduce the dark current of the signal. A UV band-pass filter (UG5 Schott) in the light beam reduced stray light in the spectrograph.

[19] The DOAS measurements employed the multichannel scanning technique (MCST) [*Brauers et al.*, 1995; *Knoll et al.*, 1990; *Stutz*, 1996]. Spectra were taken in the following sequence: (1) The measured light intensity was maximized by an automatic telescope alignment routine. (2) An absorption spectrum was measured; the integration time of 2 to 60 s was chosen according to the visibility. (3) A

Table 1. Overview of the Measured Species and the Observed Mixing Ratios

Species	Wavelength Window, nm	Absorption Cross Section	Average Day 0700–2100, ppb[a]	Average Night 2100–0700, ppb	Maximum Mixing Ratio, ppb	Detection Limit, ppb
HONO	375–336	[*Stutz et al.*, 2000]	0.14	0.92	4.4 ± 0.2[b]	0.2
NO_2	375–336	[*Harder et al.*, 1997]	18.3	33.2	115.2 ± 0.6[c]	0.6
NO	–		5.1	84.30	480[d]	0.25
SO_2	322–303	[*Vandaele et al.*, 1994]	1.15	1.16	9.1 ± 0.22[e]	0.18
O_3	322–303	[*Bass and Paur*, 1985]	45	11	123 ± 9[f]	8.5
HCHO	322–303	[*Cantrell et al.*, 1990]	8.5	6.2	33.6 ± 1.8[g]	1.6

[a] All times, UTS (local − 2 hours).
[b] Recorded at 2125 on 13 May 1998.
[c] Recorded at 2108 on 13 May 1998.
[d] Recorded at 2130 on 7 May 1998.
[e] Recorded at 0847 on 19 May 1998.
[f] Recorded at 1237 on 13 May 1998.
[g] Recorded at 0832 on 13 May 1998.

background spectrum of the scattered sunlight or light from other sources was recorded by blocking the lamp. (4) Steps 2 and 3 were repeated nine times, advancing the wavelength by 0.8 nm on each repetition. In addition, Xe lamp and mercury lamp spectra were taken automatically every few hours.

2.3. Evaluation of the Spectra

[20] The evaluation proceeded in two steps. First, the 18 MCST spectra were processed. Then the resulting spectrum was analyzed following the principles of DOAS evaluation [*Platt*, 1994; *Stutz and Platt*, 1996].

[21] To process the MCST spectra, the background spectra were first subtracted from the respective absorption spectra. The nine resulting spectra were then added to each other to produce a sensitivity curve for the individual diodes. Each spectrum was divided by the diode sensitivity and then shifted back to the middle wavelength of spectrum number 5. Finally, the sum of all nine shifted spectra was calculated [*Stutz*, 1996]. After this procedure the diode sensitivity and a part of the broadband structure have been removed. This spectrum was then further analyzed by a nonlinear least squares procedure by fitting reference spectra of trace gases, the spectral structure of the lamp, and a

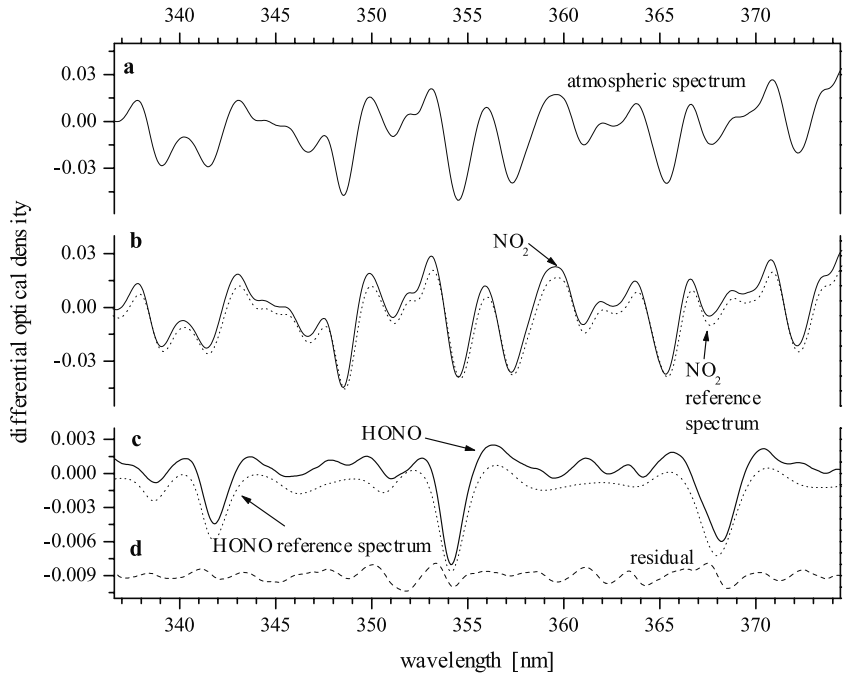

Figure 2. Example spectra (13 May 1998, 2125 UT) for the HONO and NO_2 analysis with the long-path DOAS system. Figure 2a shows the atmospheric spectrum before the evaluation. The strong absorptions of NO_2 dominate, as can be seen by comparison with the fitted NO_2 reference spectrum (dotted line in Figure 2b). Figure 2b shows a comparison of the NO_2 reference spectrum and the reference spectrum plus added residual structures. The NO_2 mixing ratio in this spectrum is (109.3 ± 0.5) ppb. A similar comparison for HONO is displayed in Figure 2c. The absorption structure of nitrous acid can clearly be identified. The HONO mixing ratio in this case was (4.4 ± 0.2) ppb. Figure 2d shows the residual structure after simultaneously removing all trace gas absorptions (dashed line). The residual of the fit is mainly due to uncorrected instrumental structures.

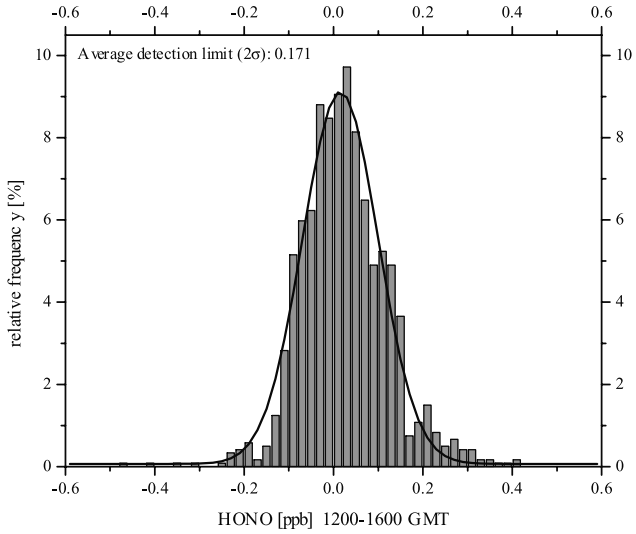

Figure 3. Frequency distribution of HONO mixing ratios during periods of large actinic flux. The relative frequency agrees well with a Gaussian curve (solid line, see text) at 15 ppt. The average error determined for each individual spectrum agrees well with the width of this distribution.

polynomial of degree eight [*Stutz and Platt*, 1996]. The concentrations of the respective species were calculated from the scaling factors of the reference spectra and the absorption cross sections. The reference spectra were calculated from literature absorption cross sections, or directly measured in the field in the case of NO_2, SO_2 and formaldehyde. In the latter case the spectra were scaled according to the literature absorption cross section. Table 1 lists the literature absorption cross section we used. An example of an analysis is shown in Figure 2. To prove the performance of our analysis, the residual spectrum after subtracting the scaled references, the scaled lamp spectrum, and the polynomial are also shown.

[22] We evaluated two separate wavelength regions in our spectrum using different combinations of reference spectra. In the 336–375 nm range we determined the concentrations of NO_2, HONO, formaldehyde, O_4, and ozone. From 303 to 322 nm we evaluated ozone, SO_2, formaldehyde, and NO_2. The error of the trace gas concentrations calculated by the least squares fitting procedure underestimates the "true" statistical error and was corrected by multiplication with a factor of 3 [*Stutz and Platt*, 1996] (all errors in this paper refer to the 1σ error).

[23] During the LOOP/PIPAPO campaign, a mean detection limit (2σ) of 200 ppt for HONO was observed (average over the complete campaign). To test the validity of the calculated detection limit, a frequency count for the HONO values measured between 1200 and 1600 UT was performed. Owing to the large actinic flux during these hours, the HONO mixing ratios are expected to lie around a few tens parts per trillon, well below our detection limit. As expected, the histogram in Figure 3 shows a normal distribution with a maximum at 15 ± 2.3 ppt. The detection limit calculated from a Gaussian fit to this graph is 0.169 ppb, which is in excellent agreement with the average of the detection limit calculated for each spectrum of 0.171 ppb.

[24] The systematic errors of the reported trace gas mixing ratios are dominated by the uncertainties of the absorption cross sections (Table 1). The uncertainty of the cross section is ±5% for HONO [*Stutz et al.*, 2000] and ±8% for NO_2 [*Harder et al.*, 1997]. The systematic error of the DOAS spectrometer was determined by *Stutz* [1996] as <3%. The total systematic error of the HONO concentration determination by DOAS is therefore <6% (NO_2: <9%).

3. Results

3.1. Meteorological Data

[25] Figure 4 gives an overview of the meteorological data in Bresso. The temperature varied between 283 and

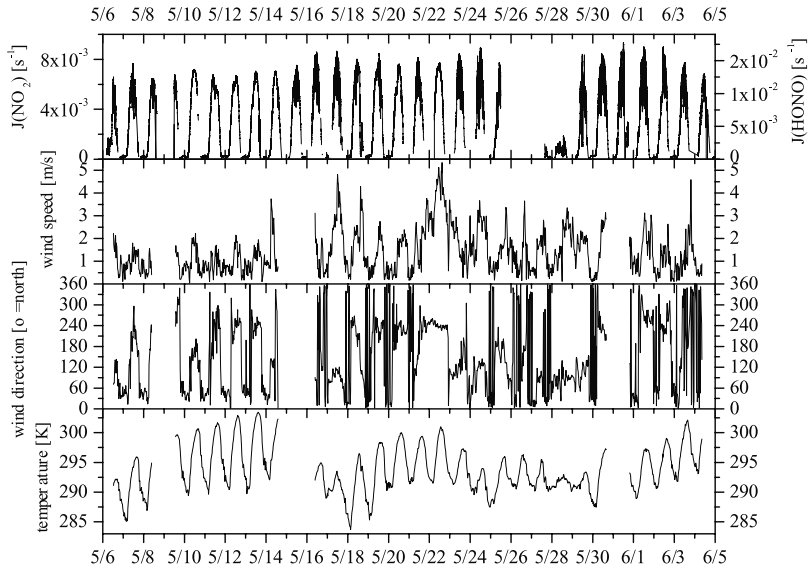

Figure 4. Temperature, wind speed and direction, and the photolysis frequencies of HONO and NO_2 for the complete campaign. The measurements were taken with the sonic anemometer. The relative humidity data were measured by A. Thielmann (personal communication, 1999).

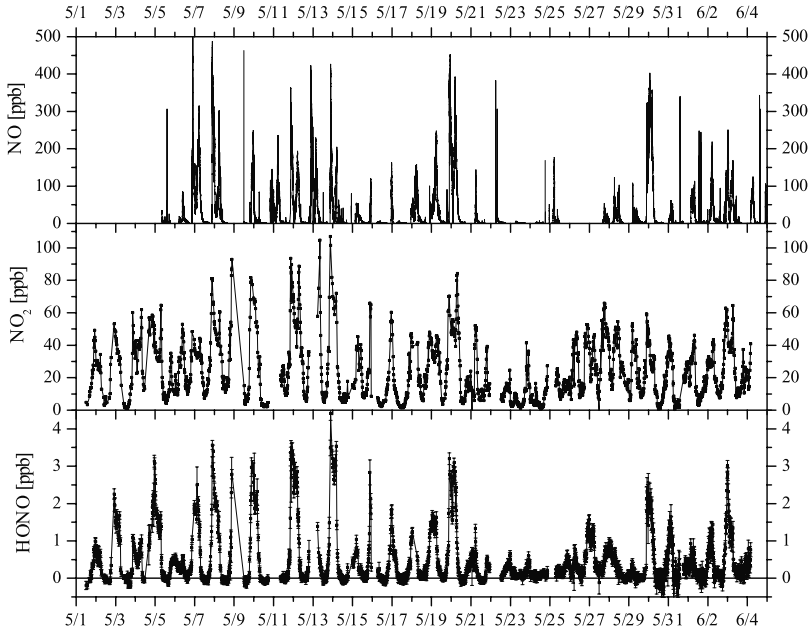

Figure 5. Time series of HONO, NO_2, and NO mixing ratios. The dotted line shows the detection limit (2σ). Only data from the upper reflector are shown. The strong diurnal cycle of HONO with a daytime minimum and nighttime maximum can be seen.

303 K, with an overall average of 293 K. The relative humidity reached 80–100% during the nights and was typically 50–60% during the day. Very moderate winds of 0.5 m s^{-1} were observed during most nights. The daytime wind speeds were higher, ~2 m s^{-1}. The wind was mainly coming from northeast and southwest. Winds directly from Milan (south = 180°) were rarely observed. Wind directions showed sudden changes, as can be seen in Figure 4. The influence of these fast changes on trace gas concentrations will be discussed later.

3.2. Trace Gases

[26] An overview of the results of the complete campaign can be seen in Figure 5 (HONO, NO_2, and NO) and Figure 6 (O_3, HCHO, and SO_2). Table 1 summarizes the detection limits, maximum, and average day and night mixing ratios.

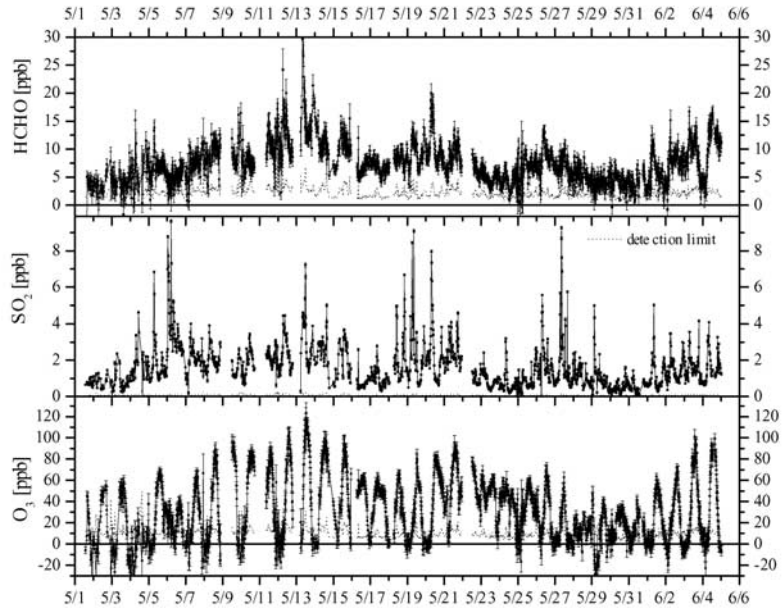

Figure 6. Overview of ozone, SO_2, and formaldehyde mixing ratio measured on the upper light path. The dotted lines show the detection limits.

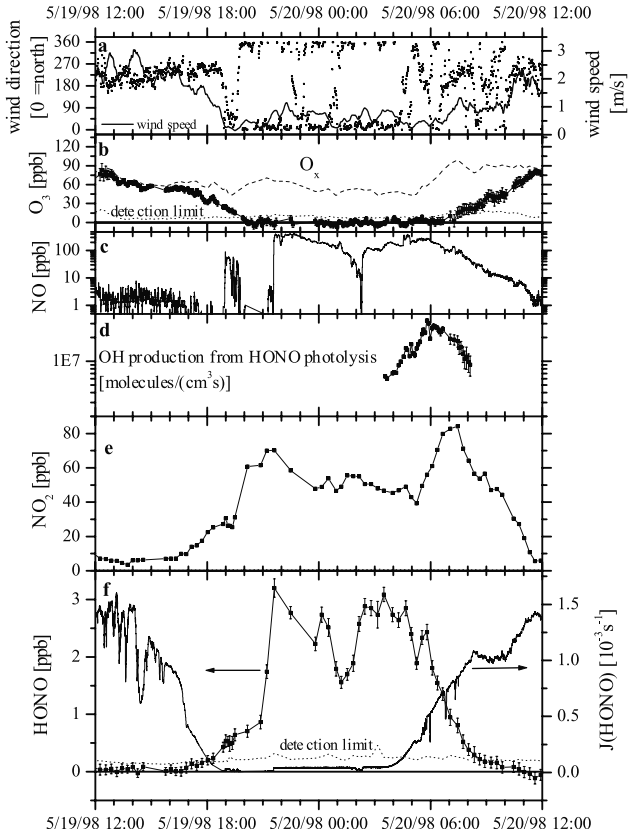

Figure 7. Data of the night of 19–20 May 1998. Figure 7a shows the wind direction (left axis) and the wind speed (dotted line, right axis). After 1800 UT the wind weakens and changes to the northerly direction. In Figure 7b the ozone mixing ratio is plotted together with Ox = NO_2 + O_3 (dashed line). The relatively constant Ox levels indicate a titration of the ozone by NO. The rapid increase of NO (Figure 7c) and NO_2 (Figure 7e) can be explained by transport of polluted air from the highway north of the site (see text). In Figure 7d the OH production from the photolysis of nitrous acid during the morning hours is shown. Figure 7f shows the HONO mixing ratios and J(HONO).

The following section will discuss the results of our trace gas measurements in detail.

3.2.1. Nitrogen Monoxide

[27] The mixing ratios of NO (Figure 5) show a very strong diurnal cycle, with the highest NO values during the night and the lowest during day. Up to 400 ppb NO were measured, indicating large sources and a shallow boundary layer during the night. The fast increase of the NO mixing ratio (for example on 19, May 2130 UT, see Figure 7), which was often observed at night is caused by transport of a polluted air mass to the site. Between 1930 and 1945 UT (UT equals local time minus 2 hours) the wind turns to northerly directions with a very low wind speed of ~0.4 m s^{-1}. The time lag between the change in the wind direction and the sudden increase of the NO mixing ratio is about 2 hours. Assuming that around 1930 UT the NO mixing ratio was still close to zero due to the titration of ozone, we estimate the distance of the NO source as ~2.8 km. The most likely source is therefore the highway running at the northern end of the airport (see Figure 1). This is also confirmed by the lower NO_x concentrations measured on the weekends (not shown).

3.2.2. Ozone

[28] Ozone mixing ratios (Figure 6) show the expected behavior in the presence of strong NO sources. Elevated ozone concentrations were observed during the day, when ozone is formed photolytically. During the night, ozone reacts with NO to generate NO_2 (see, for example, Figure 8):

$$NO + O_3 \rightarrow NO_2 + O_2. \quad (16)$$

The nighttime ozone levels were therefore often very low. The low ozone levels during the night imply that the radical levels at night are also very low since NO_3 is not formed and the production of OH by ozone + alkenes reactions is inefficient. During the day, maximum ozone mixing ratios of up to 115 ppb were observed. On the two intensive observational periods (12–14 May and 1–4 June) the highest ozone levels were observed (see Table 1 and Figure 6).

[29] The anticorrelation between ozone and NO is difficult to see in our data. While the NO monitor performs a point measurement at the southern end of the light path, the DOAS system integrates an air mass that extends 1.25 km to the north. Figure 7 illustrates this behavior. While ozone mixing ratios start to decrease steadily after the change of wind direction, NO stays constant until the air mass reaches the end of the light path and then increases suddenly. The

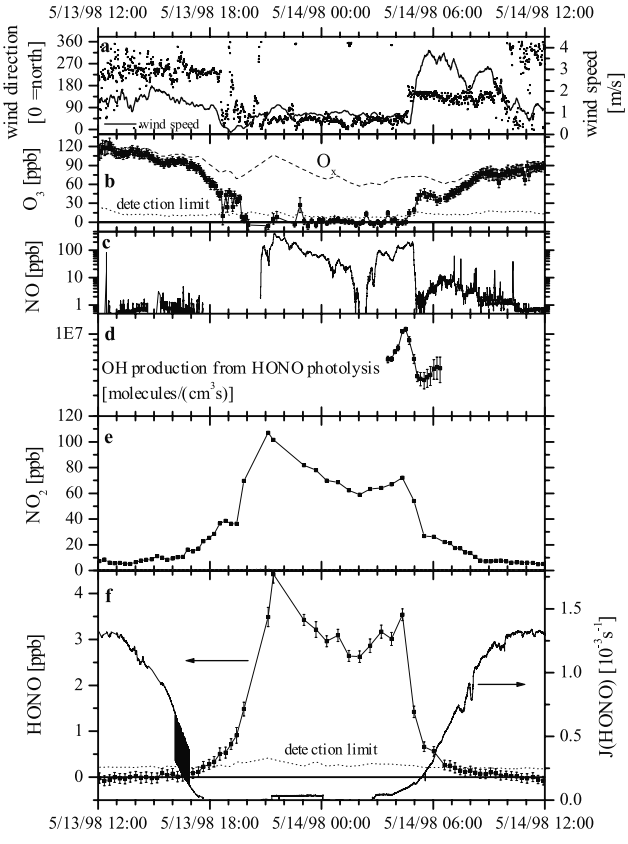

Figure 8. Data of the night of 13–14 May 1998. A similar behavior as on 19–20 May can be observed.

DOAS data are therefore smoothed when air is traveling along its light path.

3.2.3. Nitrogen Dioxide

[30] A diurnal variation similar to NO was seen for NO_2, with a nighttime maximum and a daytime minimum during large actinic flux. Typical daytime NO_2 levels of 18 ppb were observed. The nighttime mixing ratios of nitrogen dioxide vary between 20 and 115 ppb and are often similar to the maximum daytime ozone values, indicating that NO_2 at night is mainly formed by the reaction of NO with ozone. This is shown by the relatively constant O_x level ($O_x = O_3 + NO_2$) (see Figure 7 or Figure 8). The decrease of ozone is balanced by an increase of NO_2.

3.2.4. Formaldehyde

[31] Very high HCHO values of up to (33.6 ± 1.8) ppb (see Figure 6 and Table 1) were observed during PIPAPO. The highest mixing ratio of formaldehyde occurred during 13 May simultaneously with the highest ozone levels of the campaign. Typically, HCHO was around 10 ppb. The high HCHO levels indicate the high primary VOC reactivity.

3.2.5. Sulphur Dioxide

[32] SO_2 mixing ratios varied between 0.2 and 9 ppb. No clear diurnal cycle was seen for SO_2. This is in contrast to the observed NO_x levels, which are much higher during the night. It therefore seems to be likely that SO_2 is emitted by sources which are not close to the site, and that transport processes dominate SO_2 levels.

3.2.6. Nitrous Acid

[33] Mixing ratios of HONO of around 3 ppb were observed on many nights. The maximum mixing ratio measured was 4.4 ppb (see Table 1). The highest HONO was observed on nights with high NO_2. The nitrous acid mixing ratios increased steadily after sunset and often reached a relatively constant HONO/NO_2 ratio of about 5% with sporadic maximum peaks of 7%. As discussed above, two sources of HONO are probably present in Milan, direct emission and heterogeneous formation in the presence of NO_2.

[34] To estimate the conversion frequency from NO_2 into nitrous acid by reaction (12) during the night, we chose a night with low NO mixing ratios of about 10 ppb, leading to less than 65 ppt of direct HONO [*Ackermann*, 2000]. The HONO mixing ratio (Figure 9) increases steadily after sunset and reaches a maximum after midnight. We determined the HONO formation by assuming a linear increase of its mixing ratio during a time interval ($t_2 - t_1$). Since the mechanism summarized in reaction (12) is first order in NO_2, the HONO formation is proportional to the NO_2 concentration. We also assumed that the conversion frequency does not depend on gas phase water as suggested by *Kleffmann et al.* [1998]. The average nighttime conversion frequency was determined by:

$$\overline{F_{HONO,\ night}} = \frac{[HONO](t_2) - [HONO](t_1)}{(t_2 - t_1)[NO_2]_{night}}. \qquad (17)$$

The calculated value was (0.012 ± 0.005) (ppb HONO)/(h(ppb NO_2)). To calculate the direct emission of HONO, we assumed a HONO/NO_x emission rate of 0.65%, as determined by *Ackermann* [2000].

[35] To estimate the source strength of nitrous acid during the day, we assumed the conversion frequency to be the same as in the night. This means that nitrous acid is formed during the day by the same mechanism as during the night, but owing to the fast photolysis into OH (reaction (1), τ_{HONO} = 9.5 min (1200 UT)) it never exceeds the detection limit.

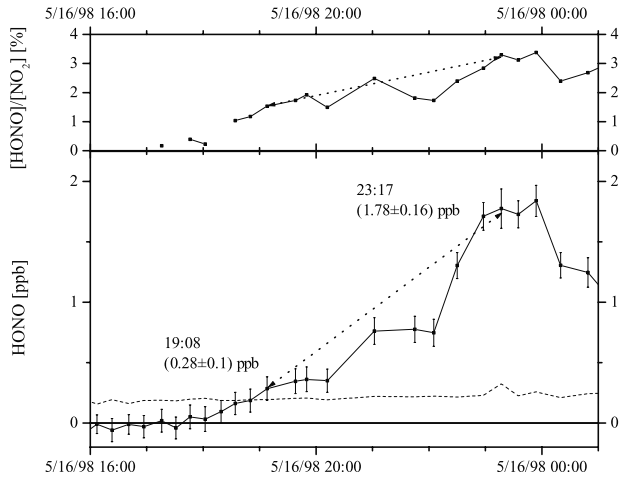

Figure 9. Formation of HONO during the night of 16 May. The lower graph shows a monotonic increase of HONO from 1908 to 2317. The upper graph shows the corresponding increase in the HONO/NO_2 ratio. The data we used to determine the conversion frequency of NO_2 to HONO are indicated with dotted lines with arrows.

3.3. Daytime Nitrous Acid

[36] The measurements of daytime HONO allow us to investigate whether the conversion of NO_2 to HONO also proceeds during the day. The comparison of the observations to calculated steady state HONO mixing ratios will show whether the heterogeneous NO_2 to HONO conversion also has to be considered as a HONO source during the day. We will concentrate here on two days, May 6 and May 18, where HONO was observed at levels above the detection limit.

3.3.1. Results for 6 May

[37] The photolysis rates during the morning hours of 6 May (see Figure 10) stayed low until 1100 UT, owing to a dense cloud cover. During this time the nitrous acid mixing ratio reached maximum values of (0.63 ± 0.07) ppb at 0959 UT. The three main HONO absorption structures at 341.7, 354.1, and 368.1 nm can be clearly identified in this particular spectrum (Figure 11). The mixing ratios and photolysis rates of the other trace gases at this time were: NO_2 = 47.3 ± 0.17 ppb, NO = 46 ± 0.1 ppb, O_3 < 5 ppb, HCHO = 5 ± 0.8 ppb, $J_{O1D} = 4.7 \pm 0.7 \times 10^{-6}\ s^{-1}$, $J_{NO2} = 1.7 \pm 0.25 \times 10^{-3}\ s^{-1}$.

[38] Since the time from sunrise to about 1000 UT is longer than the actual photolytic lifetime of 1–1.5 hours, we assume that HONO is in a pseudosteady state at this time. To test if the observed daytime HONO mixing ratios can be explained by the equilibrium between reactions (1) and (10), the OH concentration during the morning of 6 May has to be estimated. Using the expression for the dependence of the OH concentration on solar UV and NO_2 by *Ehhalt and Rohrer* [2000],

$$[OH] = a(J_{O^1D})^{\alpha}(J_{NO_2})^{\beta}\frac{bNO_2 + 1}{cNO_2^2 + dNO_2 + 1} \qquad (18)$$

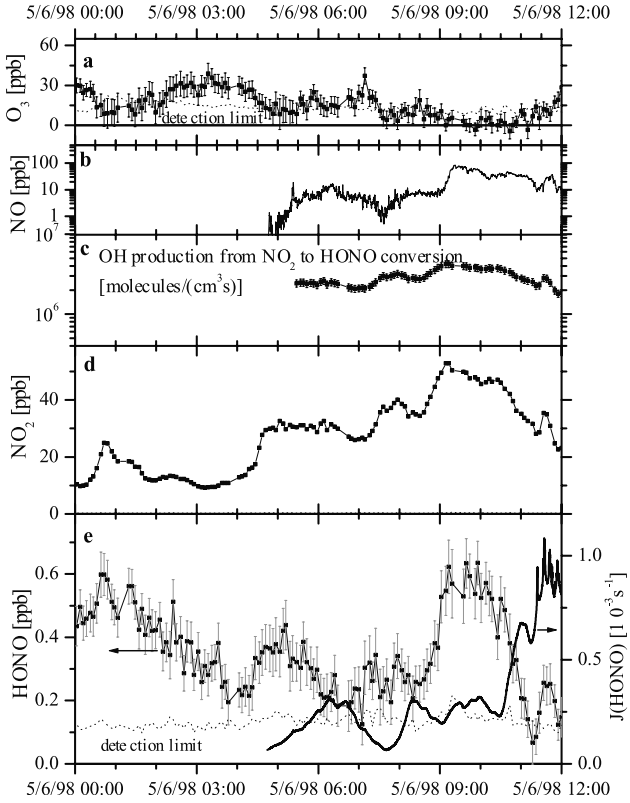

Figure 10. The importance of nitrous acid as a daytime OH source can be seen during time periods with low actinic flux. The morning of 6 May is shown here as an example. Nitrous acid stayed above the detection limit with mixing ratios of up to (0.63 ± 0.07) ppb for most of the morning.

($\alpha = 0.83$, $\beta = 0.19$, $a = 4.1 \times 10^9$, $b = 140$, $c = 0.41$, and $d = 1.7$), we calculate an OH concentration of $(3.5 \pm 0.6) \times 10^5$ molecules cm^{-3}. Since this equation was derived for a rural area, it is not clear if it is also applicable for the polluted conditions in Milan. The presence of HONO in polluted areas, for example, can increase the OH concentration, and equation (18) most likely underestimates the OH levels. We therefore also made a pseudosteady state calculation of the OH concentration. The OH production was estimated from the measured O_3, HCHO, HONO, and VOC concentrations and the measured or modeled photolysis rates. A more detailed discussion of the individual OH source terms will follow in the next section. The loss of OH was assumed to proceed via its reaction with NO_2, NO, and the limited number of hydrocarbons that were measured [*Grüebler*, 1999]. For the morning of 6 May we estimated an OH concentration of 3.5×10^5 molecules cm^{-3}. Since we did not include all OH loss processes, particularly reactions with other hydrocarbons, the calculated OH loss rate is most likely too small and the estimated OH concentration is an upper limit. The uncertainty of this value is difficult to determine, since it is probably dominated by unknown OH loss reactions. Assuming only the uncertainties of the input data, we derive an error of $\sim 1 \times 10^5$ molecules cm^{-3}. The value derived by equation (18) and our upper estimate agree surprisingly well. In the following we will therefore use an upper limit for the OH concentration of $(3.5 \pm 1) \times 10^5$ molecules cm^{-3}.

[39] We calculated an upper limit HONO steady state mixing ratio based only on the following reactions, which do not include a conversion of NO_2 to HONO:

$$\mathrm{HONO} + h\nu \rightarrow \mathrm{OH} + \mathrm{NO} \quad (300\ \mathrm{nm} < \lambda < 405\ \mathrm{nm}), \qquad (1')$$

$$\mathrm{OH} + \mathrm{NO} \rightarrow \mathrm{HONO} \quad k_{(10)} = 3.9 \times 10^{-12}\ \mathrm{cm^3\ molecule^{-1}\ s^{-1}}, \qquad (10')$$

$$\mathrm{HONO} + \mathrm{OH} \rightarrow \mathrm{NO_2} + \mathrm{H_2O} \qquad (19)$$
$$k_{(19)} = 4.5 \times 10^{-12}\ \mathrm{cm^3\ molecules^{-1}\ s^{-1}}.$$

[40] The steady state HONO mixing ratio based on these reactions is (0.36 ± 0.11) ppb. This value is lower than the observed value of (0.62 ± 0.07) ppb. It therefore seems likely that an additional HONO source is present during the day. We tested this hypothesis by assuming a daytime production by the same mechanism as during the night:

$$P_{\mathrm{HONO,day}}(t) = \overline{F_{\mathrm{HONO,night}}}[\mathrm{NO_2}](t). \qquad (20)$$

We also used typical emission data of NO_x and the HONO/NO_x emission ratio determined by *Ackermann* [2000] to approximate the direct emission of HONO. The emission of HONO was calculated from the total Milan emission strength of NO_x (3.88×10^{12} molecules cm^{-2} s^{-1} [*Staffelbach et al.*, 1997b]), the assumption that 0.65% of the NO_x emission is nitrous acid [*Ackermann*, 2000], and a mixing height of 200 m. The mixing height was chosen to be 200 m because HONO emitted at the ground is rapidly photolyzed during its vertical transport. Most of the HONO will not reach heights above 200 m.

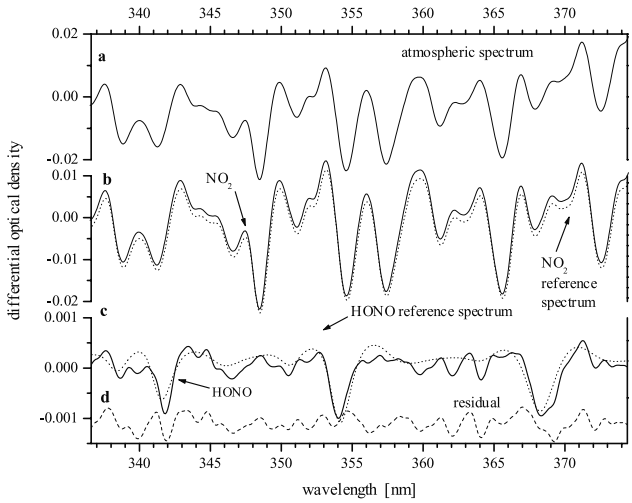

Figure 11. Daytime spectrum of nitrous acid for 6 May. The mixing ratio that was found in this spectrum was (0.63 ± 0.07) ppb. Figure 11a shows the atmospheric spectrum. Its structure is dominated by the absorption of NO_2 (see Figure 11b) with a mixing ratio of (47.3 ± 0.17) ppb. In Figure 11c the HONO absorption structure can be seen. All three absorption bands can be easily identified. The dotted line shows the HONO reference spectrum. Figure 11d plots the residual after removing all absorbers.

[41] Assuming a pseudosteady state, we derived an expression for HONO adding the following reactions to the above described reactions:

$$\begin{aligned} NO_2 + NO_2 + H_2O &\rightarrow HONO + HNO_3 \quad P_{HONO,day(t)} \\ &\rightarrow \quad HONO \quad E(HONO) = \text{direct emission.} \end{aligned} \tag{12'}$$

[42] The steady state expression of the daytime HONO concentration is then given by

$$[HONO] = \frac{\left\{[OH][NO]k_{(10)} + P_{HONO,day}(NO_2)[NO_2]E(HONO)\right\}}{\left(J_{HONO} + [OH]k_{(20)}\right)^{-1}}. \tag{21}$$

Using the same OH concentrations as above, plus the additional production through NO_2-HONO conversions, and taking direct emission into account, we calculate a steady state mixing ratio of (0.80 ± 0.25) ppb. This is in good agreement with the measurement of (0.62 ± 0.07) ppb considering that our OH concentration was an upper estimate.

[43] This simple calculation shows that the conversion of NO_2 to HONO also proceeds during the day. The observations during the night can be used to approximate the daytime HONO formation and the subsequent OH production. Using expression (21) we also estimated the HONO mixing ratio during a sunny day. On 20 May at 1100 UT we observed the following trace gas mixing ratios: 5.9 ppb, for NO and 18.9 ppb for NO_2. The HONO photolysis rate was J_{HONO} (0.00134 s^{-1}). The OH concentration was estimated to 6×10^6 molecules cm^{-3}. This value agrees well with OH levels reported by *George et al.* [1999] for the polluted Los Angeles atmosphere. The HONO mixing ratio in this case reaches a maximum of 120 ppt, which is below the detection limit of our system.

3.3.2. Results for 18 May

[44] At 1415 UT on 18 May J(HONO) dropped within 45 min from 1.36×10^{-3} s^{-1} (τ_{HONO} = 13 min) to 9.8×10^{-5} s^{-1} (τ_{HONO} = 210 min) (see Figure 12). Simultaneously with the decrease of J(HONO) the mixing ratio of nitrous acid increases to a maximum value of (0.31 ± 0.1) ppb. A quantitative analysis of these data is difficult since the event is shorter than the time to establish a steady state among HONO, OH, and NO. The NO mixing ratio around this time was around 1 ppb, and we estimated an upper limit for OH from our calculations of 1.5×10^5 molecules cm^{-3}. At these levels the steady state HONO mixing ratio considering only reactions (1), (10), and (19) would have been around 0.17 ppb. Although this is only a rough estimate, it confirms our conclusions for 6 May that a formation of HONO beyond the OH + NO reactions occurs during the day.

[45] The daytime formation of HONO will ultimately lead to a net source of OH radicals. The impact of this source will be discussed in the next section.

3.4. Quantification of the Hydroxyl Radical Production Rates

[46] To assess the importance of HONO photolysis as an OH source, we calculated the OH production from other important formation mechanisms. From our measurements we were able to quantify the OH formation rates from HONO, ozone, and formaldehyde photolysis. A lower limit from the ozonolysis of alkenes was derived using hydrocarbon data from *Grüebler* [1999]. The formation from the photolysis of higher aldehydes was estimated from typical values found in the Milan area. Other sources appear to be unimportant. The following section describes our calculations and discusses the results for the individual mechanisms. We concentrate here on two sunny days during the campaign, 14 and 20 May. As will be explained later, our discussion is restricted to the lowest 200 m of the troposphere.

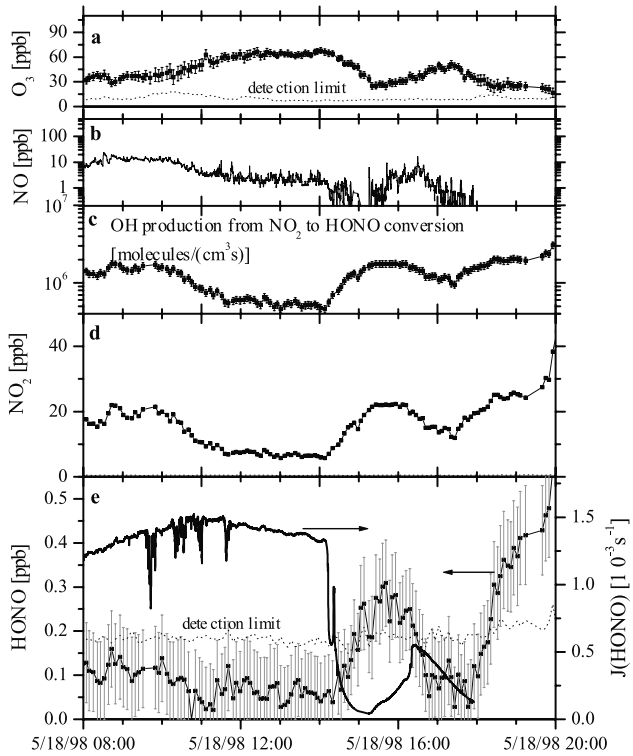

Figure 12. HONO mixing ratios during a fast decrease of the actinic flux on the afternoon of 18 May. The highest HONO mixing ratio during this event was (0.31 ± 0.1) ppb. The fast increase of nitrous acid directly correlated with the decrease of its photolysis rate can clearly be seen.

3.4.1. HONO Photolysis

[47] The OH formation rate by HONO photolysis, P_{OH}(HONO), was derived in three different ways, depending on the time of day. In the early morning we used our measurements of HONO and J(HONO) to calculate the OH formation directly via

$$P_{OH}(HONO) = J(HONO)[HONO]$$

The photolysis rate of HONO, J(HONO), was obtained using the measured $J(NO_2)$ values and the conversion equation derived by *Kraus and Hofzumahaus* [1998]:

$$J(HONO) = 0.189\, J(NO_2) + 8.433 \times 10^{-2}\, J(NO_2)^2 \tag{22}$$

An overview of the measured $J(NO_2)$ and J(HONO) photolysis rates calculated with the above expression can

be seen in Figure 4. The OH formation rates calculated from the measured HONO concentrations and J(HONO) in the early morning for 14 and 20 May are shown in Figures 7 and 8. The morning photolysis can form up to $1-3 \times 10^7$ OH cm^{-3} s^{-1} and lasts about 3–5 hours after sunrise, depending on the actinic flux.

[48] During the day, the formation of HONO through reaction (12) was estimated according to equation (17) by extrapolating our observed nighttime NO_2 to HONO conversion. We also included the direct emission of HONO. As described above, the direct emission was estimated from the average NO_x emissions in Milan of 3.88×10^{12} molecules cm^{-2} s^{-1} [*Staffelbach et al.*, 1997a] and a mixing height of 200 m. Both daytime HONO formation mechanisms are quantitatively converted to OH radicals during the day. We have not considered the reaction of OH + NO as a HONO source here since it does not contribute to a net OH formation. The OH formation rates from the daytime NO_2 to HONO conversion for the days when we observed HONO above the detection limit are illustrated in Figures 10 and 12. It can be seen that daytime OH formation rates from this process can reach up to 4×10^6 OH cm^{-3} s^{-1}. It should be noted that the estimate of the direct emission is assumed to be constant and does not reflect diurnal variations in NO_x emissions.

[49] It should be noted that HONO photolysis is important only in the lowest few hundred meters of the atmosphere. While morning photolysis is often restricted to the nighttime boundary layer, the fast photolysis later during the day does not permit a transport of HONO into the upper part of the daytime boundary layer. We will therefore limit our discussion of the OH formation processes to the lowest part of the troposphere.

[50] Figure 13 shows the early morning and daytime contribution of HONO photolysis to the OH formation for 14 and 20 May. On these two days the contribution from the daytime HONO sources is around 5×10^5 molecules cm^{-3} s^{-1} at noon. This value is lower than the values listed above owing to lower NO_2 concentration.

[51] The 24 hour integrated values of the three contributions are summarized in Table 2. On 20 May, for example, the morning peak due to the photolysis of the HONO dominates the 24 hour contribution of HONO photolysis to the OH budget. The formation of HONO during the day and the direct emission are responsible for $(5.5 \pm 2) \times 10^{10}$ molecules cm^{-3} and 7.3×10^{10} molecules cm^{-3} respectively. It should be noted that owing to the relatively fast photolysis of HONO compared to other HONO loss paths, the HONO formed during the night will be totally photolyzed after sunrise, even during cloudy periods. The same is true for the other contributions except for the last few hours of the day, when the formed HONO will increase the nighttime levels. The 24 hour integrated OH production by HONO photolysis is therefore relatively independent from the actinic flux.

3.4.2. Ozone Photolysis

[52] The OH formation rate by ozone photolysis at wavelengths below 319 nm, $J(O^1D)$, followed by the reaction of $O(^1D)$ with water (reactions (2) and (3)), was calculated by

$$P_{OH}(O_3) = 2J(O^1D)[O_3] \quad (\% \text{ of } O^1D \text{ going to OH})$$

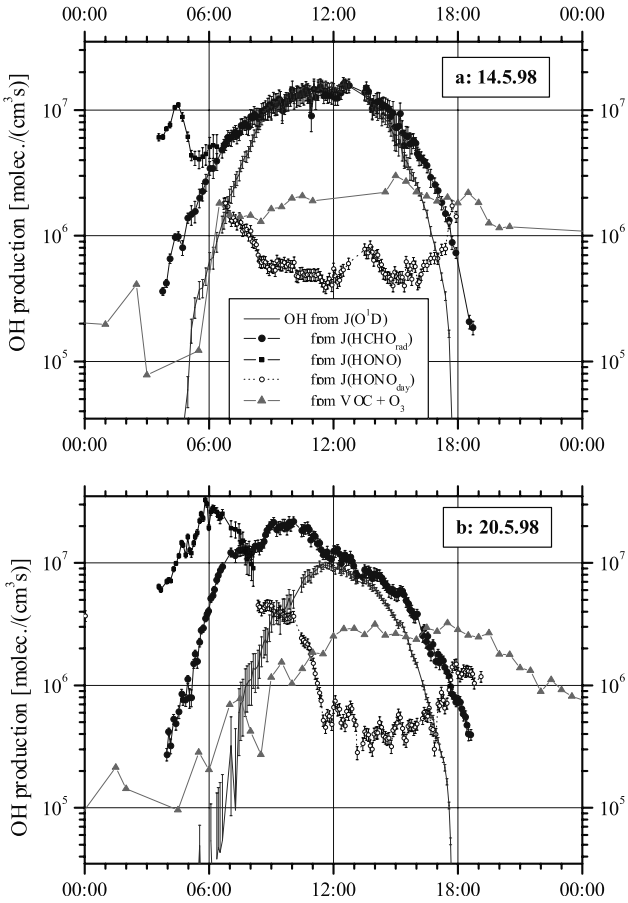

Figure 13. Comparison of four different OH-radical-producing processes for (a) 14 May 1998 and (b) 20 May 1998. The data are plotted on a logarithmic scale for a better overview. The impact of HONO photolysis on the OH formation in the early morning hours can be easily seen. The estimated daytime OH production from HONO (see text) is shown with a dotted line. See colored version of this figure at back of this issue.

Since no direct measurements were available, we applied a radiative transfer model to derive $J(O^1D)$. We used the STAR model developed by *Ruggaber et al.* [1994]. The agreement between the model values and measurements for $J(O^1D)$ was found to be better than 90% during the Berlin Ozone Experiment (BERLIOZ) field campaign [*Alicke et al.*, 2002].

[53] For PIPAPO we concentrated on mostly sunny and cloud-free days. The model input values for the vertical column of pressure, temperature, water vapor, aerosol distribution, NO_2, SO_2, and O_3 were taken for a typical spring/summer day in Europe. The ground was assumed to be isotropic, consisting mainly of grass (albedo: 0–0.27 depending on the wavelength). We validated the model results by comparing the $J(NO_2)$ with the measured values. The agreement between model and measurement is on average better than 96%. The uncertainty of the $J(NO_2)$ filter radiometer is ±15%. The excellent agreement for $J(NO_2)$ shows that the model is indeed calculating reasonable values for Milan. Nevertheless we assumed a conservative error for modeled $J(O^1D)$ of ±15%. We used relative humidity (A. Thielmann, personal communication, 1999),

Table 2. Overview of the Integrated Morning and Daytime OH Production by HONO Photolysis

Date	Morning OH Peak From HONO Photolysis 10^{10} molec. cm^{-3}	Daytime HONO = Daytime OH From HONO Photolysis 10^{10} molec. cm^{-3}	Daytime OH From the Photolysis of Directly Emitted HONO 10^{10} molec. cm^{-3}
14 May 1998	7.7 ± 0.7	2.7 ± 1.0	~7.3
20 May 1998	25.7 ± 3.2	5.5 ± 2.0	~7.3

and temperature to calculate the absolute water concentration and the branching ratio between reactions (3) and (4). The average fraction of O(^{1}D) reacting with water to OH over the complete campaign was 12.1%, with variations from 8% to nearly 18%. Together with the measured O_3 concentration and the modeled photolysis rate $J(O^1D)$, we then calculated the amount of OH produced according to reactions (2)–(4). The OH production by ozone photolysis shows the typical maximum during the highest UV radiation around noon of $1–2 \times 10^7$ molecules cm^{-3} s^{-1}, and a minimum during the night (see Figure 13).

3.4.3. HCHO Photolysis

[54] The OH production by the photolysis of formaldehyde was calculated by assuming that the HO_2 produced by reaction (5) followed by reactions (7) and (8) is immediately converted into OH by reaction (9):

$$P_{OH}(HCHO) = 2\,J(HCHOrad)[HCHO]$$

[55] The rate-limiting step is the photolysis of HCHO, with a lifetime at noon of about 10 hours. The faster step, the reaction of HO_2 with NO, in the presence of typical NO daytime mixing ratios in the range of 0.5–2 ppb, leads to a lifetime of 10–2.5 s. On 20 May the mixing ratio of NO dropped slowly from morning peak values of 390 ppb (0445 UT, $\tau_{HO2} = 0.01$ s) to mixing ratios around 10 ppb ($\tau_{HO2} = 0.45$ s) during the peak OH production from the HCHO photolysis at 1000 UT. The lower NO mixing ratios in the afternoon of about 0.5 ppb led to a HO_2 lifetime which is still much faster than HCHO photolysis. In Figure 14 the lifetime of HO_2 for the reaction with NO is plotted together with the modeled photolysis frequency and the measured formaldehyde mixing ratios. The production of OH by HCHO photolysis is shown as well. As can be seen on 20 May, the lifetime of HO_2 is very low owing to the higher NO concentration. In general, in the presence of NO mixing ratios larger than ~10 ppt, as is always the case during our study, sources of HO_2 are, in effect, sources of OH [*Finlayson-Pitts and Pitts*, 2000]. As in the case of ozone photolysis, no direct measurement of J(HCHO) was available, and we used the radiative transfer model described above to calculate J(HCHO). The agreement between the model values and measurements for $J(HCHO_{rad})$ was around 96% during the BERLIOZ field campaign. Nevertheless, we assumed a conservative error for modeled $J(HCHO_{rad})$ of ±15%.

[56] Figure 14a shows the formation rate of OH radicals from HCHO photolysis for May 20. The formation rate roughly follows actinic flux, reaching a peak value of 2×10^7 molecules cm^{-3} s^{-1} around 1000 UT, which is caused by the much higher HCHO levels in the morning.

3.4.4. Photolysis of Higher Carbonyl Compounds

[57] Besides formaldehyde a number of other oxygenated hydrocarbons form HO_2 or OH radicals upon photolysis. Since those compounds are formed in excess of the OH that is recycled after the oxidation of their precursors, they can be regarded as a net OH source. A number of these carbonyls were measured sporadically during PIPAPO. The sparse data do not allow an accurate quantification, but they are enough to yield an estimate of a lower limit. Not all carbonyls that can contribute to this OH source can be quantified. This source could therefore be considerably larger.

[58] The following species were measured in Bresso on one or two days of the study. Details of the measurements were given by A. Neftel and C. Spirig (LOOP/PIPAPO database, 1999). We used the following typical daytime values: acetaldehyde, 4ppb; propanal, 0.4 ppb; acetone, 20 ppb, methylglyoxal, 0.075 ppb; and glyoxal, 0.1 ppb.

[59] The photolysis rates were again derived from our radiative transfer model as described above. Photolysis of acetaldehyde and acetone contributes around 4.5×10^5 molecules cm^{-3} s^{-1} at noon, while methylglyoxal and glyoxal contribute around $1–2 \times 10^5$ molecules cm^{-3} s^{-1}. The total contribution of the photolysis of carbonyls we have considered at noon is 1.5×10^6 molecules cm^{-3} s^{-1}.

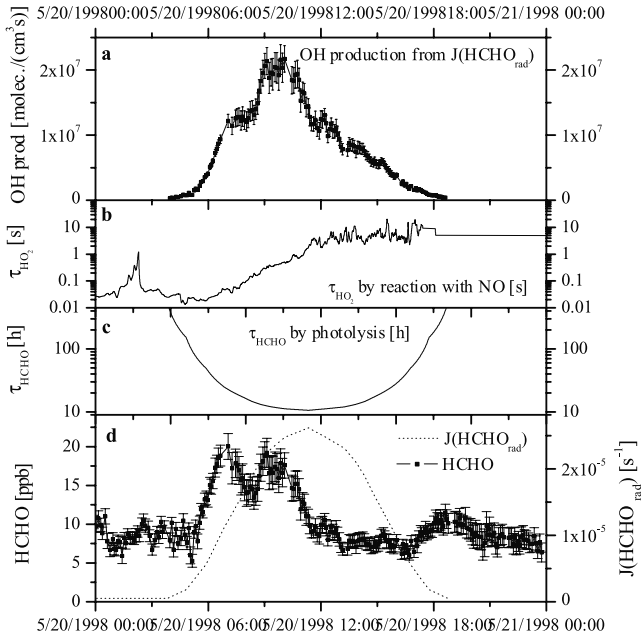

Figure 14. Figure 14a shows the production of hydroxyl radicals by the photolysis of formaldehyde, and the immediate reaction with NO afterward. The lifetime of HO_2 due to reaction with NO (reaction (9)), and due to photolysis are shown in Figures 14b and 14c, respectively. The diurnal variation of HCHO can be seen in Figure 14d (left axis), together with its photolysis frequency $J(HCHO_{rad})$ (right axis).

Table 3. Overview of All Volatile Organic Compounds Used in the Calculations Including Their Reaction Constants and OH Formation Yields

Species[a]	$K_{O3} \times 10^{-18}$, cm^3 $molec^{-1}s^{-1}$	OH Formation Yield[b]	Average Mixing Ratio Whole/20.5,[c] ppb	% of Each VOC on Total VOC → OH production[d]
i/1-Butene	9.64	0.29 ± 0.04	0.17/0.54	0.1
1,3-Butadiene	6.30	0.13 ± 0.03		
Isoprene	12.80	0.13 ± 0.03	0.15/0.28	1
trans-2-Pentene	160.00	0.47	0.22/0.42	35
2-Methyl-2-butene	403.00	0.89 ± 0.4	0.11/0.16	53
Styrene	17.00	0.07	0.0025/0.01	0.01
cis-2-Pentene	140	0.3	0.15/0.34	11

[a] Measurements by *Grüebler* [1999].
[b] If no error for the OH formation yield is given, there was no error calculation in the literature. For a recent review see *Paulson et al.* [1999].
[c] Average over the whole campaign is given first, then the average for May 20.
[d] Average for May 20, 1998.

Integrated over a 24 hour period, the photolysis of the considered carbonyls form ~1 ppb OH radicals.

3.4.5. Reaction of Alkenes With Ozone

[60] The OH production from the reaction of ozone with alkenes, as recently reviewed by *Paulson et al.* [1999], was estimated on the basis of our ozone data and measurements of different alkenes (C5 or larger) by *Grüebler* [1999]. Table 3 lists the compounds with the largest contribution to the OH formation. As expected at an urban site, high amounts of anthropogenic VOCs were present. Table 3 also lists the rate constants of the reaction of the VOCs with O_3 and the yield of OH. On the basis of these data we calculated the formation of OH radicals throughout the day:

$$P_{OH}(O_3 + \text{alkenes}) = k_{VOC+O_3}[VOC][H_3](\text{OH yield of reaction})$$

[61] Table 3 also shows the relative contribution of the individual VOCs. The most important compound is 2-methyl-2-butene, with a contribution of 54% to this formation mechanism, followed by trans-2-pentene (35%) and cis-2-pentene (11%). Since our measurements and calculation did not consider all alkenes that might have been present, this represents only a lower limit of the formation mechanism.

[62] This OH production mechanism is independent of actinic flux. It therefore proceeds throughout the night if ozone is present. Our measurements show that often the ozone concentrations at night are very low and little OH is produced. Nevertheless, on certain nights, when NO_x levels were low, production rates of $1-2 \times 10^6$ OH molecules s^{-1} were observed (e.g. 20 May, see Figure 13). During the day, typical OH production rates of 2×10^6 molecules cm^{-3} s^{-1} were observed.

3.4.6. Reaction of NO_3 With Alkenes

[63] Although NO_3 was not measured during the campaign, the low ozone and high NO levels show that NO_3 concentrations should be very low. The lifetime of NO_3 in the presence of 10 ppb NO is only 0.15 s. The formation of OH by the reaction of NO_3 with VOCs is therefore unimportant in the polluted atmosphere of Milan.

3.5. Comparison of OH Sources

[64] Figure 13 compares the diurnal variation of the OH formation rates for May 14 and May 20. We have omitted the curve for the photolysis of carbonyls since we assumed constant carbonyl concentrations and, therefore, the formation rate follows the photolysis.

[65] Both graphs show a similar trend for the individual contributions. OH production from ozone photolysis closely follows actinic flux, showing a maximum around noon. A similar trend can be observed on 14 May for formaldehyde photolysis. As expected, HCHO photolysis starts earlier in the morning and lasts longer in the evening. The noontime OH production rate on 14 May is similar for both contributions. On 20 May however, the maximum OH formation from HCHO photolysis occurs at 1000 UT. This can be explained by the higher HCHO levels at that time. This maximum is approximately twice as high as the noon values on both days.

[66] The formation of OH from ozonolysis of alkenes is insignificant during the morning in a polluted environment owing to the low ozone concentrations. It becomes more important in the evening while there is still ozone present but the actinic flux is zero. It is the only OH source after sunset.

[67] A very different diurnal trace was observed for HONO photolysis. On 14 May a maximum was observed at 0500 UT. This morning peak lasted for about 4 hours and decreased rapidly to a typical daytime value. The size of the morning maximum of $(1.1 \pm 0.2) \times 10^7$ molecules cm^{-3} s^{-1} is comparable to the noon formation rate from ozone photolysis. Daytime formation rates on 14 May are 50 times lower than the other sources, and are not very important. We observed a different behavior on 20 May. The maximum hydroxyl radical production rate by nitrous acid photolysis is $(3.2 \pm 0.4) \times 10^7$ molecules cm^{-3} s^{-1}, which is even higher than the OH production from the photolysis of ozone at noon of $(1.0 \pm 0.12) \times 10^7$ molecules cm^{-3} s^{-1}. The morning OH formation peak is also much wider than on 14 May. It lasts about 6 hours and drops to typical daytime levels around noon. This behavior is most likely caused by the much higher NO_2 mixing ratios later in the morning. While NO_2 drops to 10 ppb at 0800 UT on 14 May, it is still around 50 ppb on 20 May. It is possible that the much lower wind speeds and a weaker vertical mixing on 20 May inhibited the dilution of the pollutants that accumulated during the night. Table 4 shows the magni-

Table 4. Comparison of the Different OH Production Rates

Date	Time, UT	Species	J_x, s^{-1}	[X], ppb	OH Production $\times 10^7$, molecules cm^{-3} s^{-1}
14 May 1998	0430	HONO	$(1.3 \pm 0.2) \times 10^{-4}$	3.4 ± 0.13	1.1 ± 0.2
		HCHO	$(1.4 \pm 0.2) \times 10^{-6}$	13.8 ± 1.1	0.1 ± 0.02
		carbonyls			≈0.025
		O_3	$(2.1 \pm 0.2) \times 10^{-7}$	<8[a]	<0.008[a]
		VOC			≈0.01[b]
20 May 1998	0550	HONO	$(5.4 \pm 0.6) \times 10^{-4}$	2.43 ± 0.13	3.2 ± 0.4
		HCHO	$(5.4 \pm 0.6) \times 10^{-6}$	13.2 ± 0.8	0.35 ± 0.05
		carbonlys			≈0.025
		O_3	$(1.4 \pm 0.2) \times 10^{-6}$	<8[a]	<0.05[a]
		VOC			0.03 ± 0.015

[a] Upper limit, ozone mixing ratio below detection limit of 8 ppb.
[b] Average between 0300 and 0530 UT.

tude of OH formation from the different contributions at the maximum of HONO photolysis in the early morning. The data show that the photolysis of HONO produces 1 order of magnitude more OH than any of the other mechanisms.

[68] To estimate the role of the HONO photolysis in the total number of OH radicals produced throughout the day, we integrated the OH formation rates over 24 hours (see Table 5). As postulated by *Ehhalt et al.* [1998], *Fried et al.* [1997], and *Kleinman et al.* [1995], the most important source of OH radicals in the polluted atmosphere is the photolysis of formaldehyde (reaction (5) + (7) − (9)). With a contribution of around 40% on both days, it plays the major role in Bresso. The 24 hour integral production on 14 May is $(40.2 \pm 8.0) \times 10^{10}$ molecules cm^{-3} d^{-1} and $(45.2 \pm 8.2) \times 10^{10}$ molecules cm^{-3} d^{-1} for 20 May. The photolysis of ozone is a major contributor to the OH budget on 14 May $(34.2 \pm 6.2) \times 10^{10}$ molecules cm^{-3} d^{-1}, but plays a less important role on 20 May ($(16.7 \pm 3.0) \times 10^{10}$ molecules cm^{-3} d^{-1}). The difference in the total amount of OH from ozone photolysis is mainly dominated by a much faster increase of O_3 during the morning hours of 14 May, and the higher O_3 mixing ratio at noon (99 ± 7) ppb O_3 compared to (83 ± 4) ppb ozone on 20 May).

[69] The reaction of ozone with alkenes contributes 9% and 10% of the total OH production on 14 and 20 May, respectively. The importance of this source is the formation of hydroxyl radicals during the evening and night, when it is the strongest OH source. The contribution of the photolysis of carbonyls is around 2%, and is therefore not very important. It is probable that both ozonolysis of alkenes and photolysis of carbonyls are underestimated in this calculation and that their contribution is larger.

[70] Table 5 lists two different ways to integrate the OH production by HONO photolysis. The first and second columns refer to the formation without considering direct emissions of HONO. The following two columns have this source included. We distinguish between the two cases owing to the relative uncertainty of the direct emission at our site. If the direct emission is not taken into account we find that HONO photolysis contributes $(10.5 \pm 1.2) \times 10^{10}$ molecules cm^{-3} d^{-1} to the OH formation on 14 May and $(31.2 \pm 3.7) \times 10^{10}$ molecules cm^{-3} d^{-1} on 20 May. When direct emissions are included, the contributions increase to $(17.8 \pm 1.2) \times 10^{10}$ molecules cm^{-3} d^{-1} on 14 May and $(38.5 \pm 3.7) \times 10^{10}$ molecules cm^{-3} day^{-1} on 20 May. On 14 May HONO phtoloysis is responsible for 17% of the daily OH formation if direct emissions are included in the calculation and 11% without direct emission. The contribution on 20 May is surprisingly high. The total contribution is 34% (29% without direct emission) of the total OH production. It is therefore the second most important formation process on this day.

4. Conclusions

[71] Our measurements in the strongly polluted environment of Milan, Italy show high concentrations of OH precursors such as ozone, HCHO, and HONO. Average levels of HCHO of 8.5 ppb together with high NO concentrations make the photolysis of formaldehyde the most significant OH formation process. On average, 40% of the OH radicals

Table 5. Comparison of the Integrated OH Production Over 24 Hours

		Without Direct HONO Emission		With Direct HONO Emission	
Date	Species	% of Total OH Production	OH Production $\int$24h, 10^{10} molecules cm^{-3} d^{-1}	% of Total OH Production	OH Production $\int$24h, 10^{10} molecules cm^{-3} d^{-1}
14 May 1998	O3	35	34.2 ± 6.2	33	34.2 ± 6.2
	HONO	11	10.5 ± 1.2[a]	17	17.8 ± 1.2[a]
	HCHO	41	40.2 ± 8.0	39	40.2 ± 8.0
	Carbonyls	3	2.5[b]	2	2.5[b]
	VOC + O_3	10	9.5 ± 4.7[b]	9	9.5 ± 4.7[b]
20 May 1998	O_3	16	16.7 ± 3	15	16.7 ± 3
	HONO	29	31.2 ± 3.7[a]	34	38.5 ± 3.7[a]
	HCHO	42	45.2 ± 8.2	39	45.2 ± 8.2
	Carbonyls	2	2.5[b]	2	2.5[b]
	VOC + O_3	11	11.7 ± 5.7[b]	10	11.7 ± 5.7[b]

[a] See text.
[b] Lower estimate.

formed on a clear day originate from this mechanism. In contrast to less polluted areas, the photolysis of ozone only contributes 15–30% of the daily OH formation.

[72] While the role of HCHO and ozone photolysis has been well characterized in the past, we were able for the first time to accurately quantify the contribution of HONO photolysis to the OH budget in a strongly polluted environment. Our DOAS measurements in Bresso show nighttime nitrous acid mixing ratios of up to 4.4 ppb. These levels confirm findings in other strongly polluted cities like Los Angeles. We observed HONO levels of up to 0.6 ppb on cloudy days with low actinic flux. Our calculations show these mixing ratios can only be explained if HONO formation also proceeds during the day. Our measurements also show that direct emissions of HONO play an important role in the Milan area. Using this information, we were able to calculate the OH formation rates by HONO photolysis. The morning peak, caused by the photolysis of the HONO accumulated during the night, can reach maximum values of OH formation rates that are comparable to the total OH formation rates at noon. During the first 4 to 6 hours after sunrise, HONO photolysis is by far the most important OH source in the lowest part of the troposphere. Taking direct emissions into account, HONO photolysis also impacts the daytime OH formation. Its contribution can be 17–34% of the total OH formation, similar in size to the photolysis of ozone.

[73] HONO photolysis is therefore one of the most important OH precursors in the polluted urban environment. Its inclusion in photochemical models is essential to correctly describe the chemical processes that lead to ozone formation. Since the chemistry of HONO formation is still unclear, further research is needed to determine a better mechanism that describes HONO formation in the atmosphere.

[74] **Acknowledgments.** We would like to thank Commandant Mario Quarta for his hospitality, M. Tamponi, H.-J. Veitel, M. Mössner, and K. Hebestreit for their help with the instrument, and Y. Wadia, and A. Neftel for helpful comments.

References

Ackermann, R., Auswirkungen von Kraftfahrzeugemissionen in der urbanen Atmosphäre, Ph.D. thesis, Univ. Heidelberg, Heidelberg, Germany, 2000.

Alicke, B., A. Geyer, A. Hofzumahaus, F. Holland, S. Konrad, J. Schäfer, J. Stutz, A. Volz-Thomas, and U. Platt, OH formation by HONO photolysis during the BERLIOZ experiment, *J. Geophys. Res*, doi:10.1029/2001JD000579, in press, 2002.

Ammann, M., M. Kalberer, D. T. Jost, L. Tobler, E. Rossler, D. Piguet, H. W. Gaggeler, and U. Baltensperger, Heterogeneous production of nitrous acid on soot in polluted air masses, *Nature*, *395*, 157–160, 1998.

Appel, B. R., A. M. Winer, Y. Tokiwa, and H. W. Biermann, Comparison of atmospheric nitrous acid measurements by annular denuder and differential optical absorption systems, *Atmos. Environ*, *24A*, 611–616, 1990.

Atkinson, R., and S. M. Aschmann, OH radical production from the gas-phase reactions of O_3 with a series of alkenes under atmospheric conditions, *Environ. Sci. Technol.*, *27*, 1357–1363, 1993.

Atkinson, R., S. M. Aschmann, J. Arey, and B. Shorees, Formation of OH radicals in the gas phase reactions of O_3 with a series of terpenes, *J. Geophys. Res.*, *97*, 6065–6073, 1992.

Bass, A. M., and R. J. Paur, The ultra-violet cross section of ozone, in *Proceedings of the Quadrennial Ozone Symposium*, edited by C. Zerefos and A. Ghazi, D. Reidel, Norwell, Mass., 1985.

Brauers, T., M. Hausmann, U. Brandenburger, and H. P. Dorn, Improvement of differential optical absorption spectroscopy with a multichannel scanning technique, *Appl. Opt.*, *34*(21), 4472–4479, 1995.

Brauers, T., U. Aschmutat, U. Brandenburger, H. P. Dorn, M. Hausmann, M. Hessling, A. Hofzumahaus, F. Holland, C. Plassdulmer, and D. H. Ehhalt, Intercomparison of tropospheric OH radical measurements by multiple folded long-path laser absorption and laser induced fluorescence, *Geophys. Res. Lett.*, *23*, 2545–2548, 1996.

Calvert, J. G., G. Yarwood, and A. M. Dunker, An evaluation of the mechanism of nitrous acid formation in the urban atmosphere, *Res. Chem. Interm.*, *20*(3–5), 463–502, 1994.

Cantrell, C. A., J. A. Davidson, A. H. McDaniel, R. E. Shetter, and J. G. Calvert, Temperature-dependent formaldehyde cross sections in the near-ultraviolet spectral region, *J. Phys. Chem.*, *94*, 3902–3908, 1990.

Carslaw, N., L. Carpenter, J. M. C. Plane, B. J. Allan, R. A. Burgess, and K. C. Clemitshaw, Simultaneous observations of nitrate and peroxy radicals in the marine boundary layer, *J. Geophys. Res.*, *102*, 18,917–18,933, 1997.

Chan, W. H., R. J. Nordstrom, J. G. Calvert, and J. H. Shaw, Kinetic study of HONO formation and decay reactions in gaseous mixtures of HONO, NO, NO_2, H_2O, and N_2, *Environ. Sci. Technol.*, *10*, 674–682, 1976.

Crutzen, P. J., and P. H. Zimmermann, The changing photochemistry of the troposphere, *Tellus*, *43AB*, 136–151, 1991.

Donahue, N. M., J. H. Kroll, J. G. Anderson, and K. L. Demerjian, Direct observation of OH production from the ozonolysis of olefins, *Geophys. Res. Lett.*, *25*, 59–62, 1998.

Ehhalt, D. H., and F. Rohrer, Dependence of the OH concentration on solar UV, *J. Geophys. Res.*, *105*, 3565–3571, 2000.

Ehhalt, D. H., F. Rohrer, A. Wahner, M. J. Prather, and D. R. Blake, On the use of hydrocarbons for the determination of tropospheric OH concentrations, *J. Geophys. Res.*, *103*, 18,981–18,997, 1998.

Eisele, F. L., G. H. Mount, D. Tanner, A. Jefferson, R. Shetter, J. W. Harder, and E. J. Williams, Understanding the production and interconversion of the hydroxyl radical during the Tropospheric OH Photochemistry Experiment, *J. Geophys. Res.*, *102*, 6457–6465, 1997.

Febo, A., C. Perrino, and M. Cortiello, A denuder technique for the measurement of nitrous acid in urban atmospheres, *Atmos. Environ.*, *27*, 1721–1728, 1993.

Febo, A., C. Perrino, and I. Allegrini, Measurement of nitrous acid in Milan, Italy, by DOAS and diffusion denuders, *Atmos. Environ.*, *30*, 3599–3609, 1996.

Finlayson-Pitts, B. J., and J. N. Pitts, *Chemistry of the Upper and Lower Atmosphere:Theory, Experiments and Applications*, 969 pp., Academic, San Diego, Calif., 2000.

Fried, A., et al., Photochemistry of formaldehyde during the 1993 Tropospheric OH Photochemistry Experiment, *J. Geophys. Res.*, *102*, 6283–6296, 1997.

George, L. A., T. M. Hard, and R. J. O'Brien, Measurement of free radicals OH and HO_2 in Los Angeles smog, *J. Geophys. Res.*, *104*, 11,643–11,655, 1999.

Geyer, A., B. Alicke, A. Hofzumahaus, F. Holland, S. Konrad, T. Klüpfel, H.-W. Pätz, D. Perner, A. Volz-Thomas, and U. Platt, Nighttime production of peroxy and hydroxyl radicals during the BERLIOZ campaign: Observations and modeling studies, *J. Geophys. Res*, 10.1029/2001JD000656, in press, 2002.

Goodman, A. L., G. M. Underwood, and V. H. Grassian, Heterogeneous reaction of NO_2: Characterization of gas-phase and adsorbed products from the reaction, $2NO_{2(g)} + H_2O_{(a)} \rightarrow HONO_{(g)} + HNO_{3(a)}$ on hydrated silica particles, *J. Phys. Chem. A*, *103*, 7217–7223, 1999.

Grüebler, F., Reactive hydrocarbons in the Milan area: Results from the PIPAPO campaign, Ph.D. thesis, Zürich, 1999.

Harder, J. W., J. W. Brault, P. V. Johnston, and G. H. Mount, Temperature dependent NO_2 cross section at high spectral resolution, *J. Geophys. Res.*, *102*, 3861–3879, 1997.

Harris, G. W., W. P. L. Carter, A. M. Winer, J. N. Pitts, U. Platt, and D. Perner, Observations of nitrous acid in the Los Angeles atmosphere and implications for the predictions of ozone-precursor relationships, *Environ. Sci. Technol.*, *16*, 414–419, 1982.

Harrison, R. M., and A. M. N. Kitto, Evidence for a surface source of atmospheric nitrous acid, *Atmos. Environ.*, *28*, 1089–1094, 1994.

Harrison, R. M., J. D. Peak, and G. M. Collins, Tropospheric cycle of nitrous acid, *J. Geophys. Res.*, *101*, 14,429–14,439, 1996.

Holland, F., M. Hessling, and A. Hofzumahaus, In situ measurement of tropospheric OH radicals by laser-induced fluorescence - A description of the KFA instrument, *J. Atmos. Sci.*, *52*(19), 3393–3401, 1995.

Holland, F., U. Aschmutat, M. Hessling, A. Hofzumahaus, and D. H. Ehhalt, Highly time resolved measurements of OH during POPCORN using laser-induced fluorescence spectroscopy, *J. Atmos. Chem.*, *31*(1–2), 205–225, 1998.

Jenkin, M. I., R. A. Cox, and D. J. Williams, Laboratory studies of the kinetics of formation of nitrous acid from the thermal reaction of nitrogen dioxide and water vapour, *Atmos. Environ.*, *22*, 487–498, 1988.

Junkermann, W., and T. Ibusuki, FTIR spectroscopic measurements of surface bond products of nitrogen oxides on aerosol surfaces - Implications for heterogeneous HNO_2 production, *Atmos. Environ.*, *26A*, 3099–3103, 1992.

Kaiser, E. W., and C. H. Wu, Measurement of the rate constant of the reaction of nitrous acid with nitric acid, *J. Phys. Chem.*, *81*, 187–190, 1977.

Kalberer, M., M. Ammann, F. Arens, H. W. Gaggeler, and U. Baltensperger, Heterogeneous formation of nitrous acid (HONO) on soot aerosol particles, *J. Geophys. Res.*, *104*, 13,825–13,832, 1999.

Kessler, C., and U. Platt, Nitrous acid in polluted air masses - sources and formation pathways, paper presented at the 3rd European Symposium on Physico-Chemical Behaviour of Atmospheric Pollutants, Comm. of the Eur. Commun., Varese, Italy, 10–12 April 1984.

Kessler, C., D. Perner, and U. Platt, Spectroscopic measurements of nitrous acid and formaldehyde - Implications for urban photochemistry, in *Proceedings of the 2nd European Symposium Physico-Chemical Behavior of Atmospheric Pollutants*, edited by B. Versino, pp. 393–400, Comm. of the Eur. Commun., Brussels, 1981.

Kirchstetter, T. W., R. A. Harley, and D. Littlejohn, Measurement of nitrous acid in motor vehicle exhaust, *Environ. Sci. Technol.*, *30*, 2843–2849, 1996.

Kleffmann, J., K. H. Becker, and P. Wiesen, Heterogeneous NO_2 conversion processes on acid surfaces: Possible atmospheric implications, *Atmos. Environ.*, *32*, 2721–2729, 1998.

Kleinman, L., L. Yin-Nan, S. R. Springston, J. H. Lee, L. Nunnermacker, J. Weinstein-Lloyd, Z. Xianliang, and L. Newman, Peroxy radical concentration and ozone formation rate at a rural site in the southeastern United States, *J. Geophys. Res.*, *100*, 7263–7273, 1995.

Knoll, P., R. Singer, and W. Kiefer, Improving spectroscopic techniques by a scanning multi channel technique, *Appl. Spectrosc.*, *44*, 776–782, 1990.

Kraus, A., and A. Hofzumahaus, Field measurements of atmospheric photolysis frequencies for O_3, NO_2, HCHO, CH_3CHO, H_2O_2, and HONO by UV spectroradiometry, *J. Atmos. Chem.*, *31*(1–2), 161–180, 1998.

Lammel, G., and J. N. Cape, Nitrous acid and nitrite in the atmosphere, *Chem. Soc. Rev.*, *25*(5), 361, 1996.

Lammel, G., and D. Perner, The atmospheric aerosol as a source of nitrous acid in the polluted atmosphere, *J. Aerosol Sci.*, *19*, 1199–1202, 1988.

Levy, H., Photochemistry of minor constituents in the troposphere, *Planet. Space Sci.*, *21*, 575–591, 1973.

Logan, J. I., M. J. Prather, S. C. Wofsy, and M. B. McElroy, Tropospheric chemistry: A global perspective, *J. Geophys. Res.*, *86*, 7210–7254, 1981.

Longfellow, C. A., T. Imamura, A. R. Ravishankara, and D. R. Hanson, HONO solubility and heterogeneous reactivity on sulfuric acid surfaces, *J. Phys. Chem. A*, *102*, 3323–3332, 1998.

Meller, R., and G. K. Moortgart, Temperature dependence of the absorption cross sections of formaldehyde between 223 and 323 K in the wavelength range 225–375 nm, *J. Geophys. Res.*, *105*, 7089–7101, 2000.

Mihelcic, D., D. Klemp, P. Musgen, H. W. Patz, and A. Volz-Thomas, Simultaneous measurements of peroxy and nitrate radicals at Schauinsland, *J. Atmos. Chem.*, *16*(4), 313–335, 1993.

Nguyen, M. T., R. Sumathi, D. Sengupta, and J. Peeters, Theoretical analysis of reactions related to the HNO_2 energy surface: OH+NO and H+NO_2, *Chem. Phys.*, *230*(1), 1–11, 1998.

Notholt, J., J. Hjorth, and F. Raes, Long path field measurements of aerosol parameters and trace gas concentrations—Formation of nitrous acid during foggy periods, *J. Aerosol Sci.*, *22*, S411–S414, 1991.

Notholt, J., J. Hjorth, and F. Raes, Formation of HNO_2 on aerosol surfaces during foggy periods in the presence of NO and NO_2, *Atmos. Environ.*, *26A*, 211–217, 1992.

Pagsberg, P., E. Bjerbakke, E. Ratajczak, and A. Sillesen, Kinetics of the gas phase reaction of OH + NO (+M) –> HONO (+M) and the determination of the UV absorption cross section of HONO, *Chem. Phys. Lett.*, *272*, 383–390, 1997.

Paulson, S. E., A. D. Sen, L. Ping, J. D. Fenske, and M. J. Fox, Evidence for formation of OH radicals from the reaction of O_3 with alkenes in the gas phase, *Geophys. Res. Lett.*, *24*, 3193–3196, 1997.

Paulson, S. E., M. Y. Chung, and A. S. Hasson, OH radical formation from the gas-phase reaction of ozone with terminal alkenes and the relationship between structure and mechanism, *J. Phys. Chem. A*, *103*, 8125–8138, 1999.

Perner, D., and U. Platt, Detection of nitrous acid in the atmosphere by differential optical absorption, *Geophys. Res. Lett.*, *6*, 917–920, 1979.

Pitts, J. N., H. W. Biermann, A. M. Winer, and E. C. Tuazon, Spectroscopic identification and measurement of gaseous nitrous acid in dilute auto exhaust, *Atmos. Environ.*, *18*, 847–854, 1984a.

Pitts, J. N., E. Sanhueza, R. Atkinson, W. P. L. Carter, A. M. Winer, G. W. Harris, and C. N. Plum, An investigation of the dark formation of nitrous acid in environmental chambers, *Int. J. Chem. Kinet.*, *XVI*, 919–939, 1984b.

Platt, U., The origin of nitrous and nitric acid in the atmosphere, in *Chemistry of Multiphase Atmospheric Systems*, pp. 299–319, edited by W. Jaeschke, Springer-Verlag, New York, 1986.

Platt, U., Differential optical absorption spectroscopy (DOAS), in *Monitoring by Spectroscopic Techniques*, edited by M. W. Sigrist, pp. 27–84, John Wiley, New York, 1994.

Platt, U., and F. Heintz, Nitrate radicals in tropospheric chemistry, *Isr. J. Chem.*, *34*(3–4), 289–300, 1994.

Platt, U., and D. Perner, Direct measurements of atmospheric CH_2O, HNO_2, O_3, NO_2, and SO_2 by differential optical absorption in the near UV, *J. Geophys. Res.*, *85*, 7453–7458, 1980.

Platt, U., D. Perner, G. W. Harris, A. M. Winer, and J. N. Pitts, Observations of nitrous acid in an urban atmosphere by differential optical absorption, *Nature*, *285*, 312–314, 1980.

Platt, U., G. Lebras, G. Poulet, J. P. Burrows, and G. Moortgat, Peroxy radicals from nighttime reaction of NO_3 with organic compounds, *Nature*, *348*, 147–149, 1990.

Prinn, R. G., R. F. Weiss, B. R. Miller, J. Huang, F. N. Alyea, D. M. Cunnold, P. J. Fraser, D. E. Hartley, and P. G. Simmonds, Atmospheric trends and lifetime of CH_3CCl_3 and global OH concentrations, *Science*, *269*(5221), 187–192, 1995.

Ruggaber, A., R. Dlugi, and T. Nakajima, Modeling radiation quantities and photolysis frequencies in the troposphere, *J. Atmos. Chem.*, *18*(2), 171–210, 1994.

Sakamaki, F., S. Hatakeyama, and H. Akimoto, Formation of nitrous acid and nitric oxide in the heterogeneous dark reaction of nitrogen dioxide and water vapor in a smog chamber, *Int. J. Chem. Kinet.*, *XV*, 1013–1029, 1983.

Sjödin, A., Studies of the diurnal variation of nitrous acid in urban air, *Environ. Sci. Technol.*, *22*, 1086–1089, 1988.

Sjödin, A., and M. Ferm, Measurment of nitrous acid in an urban area, *Atmos. Environ.*, *19*, 985–992, 1985.

Staffelbach, T., et al., Photochemical oxidant formation over southern Switzerland, 1, Results from summer 1994, *J. Geopys. Res.*, *102*, 23,345–23,362, 1997a.

Staffelbach, T., A. Neftel, and L. W. Horowitz, Photochemical oxidant formation over souther Switzerland, 2, Model results, *J. Geophys. Res.*, *102*, 23,363–23,373, 1997b.

Stockwell, R. W., and J. G. Calvert, The near ultraviolet absorption spectrum of gaseous HONO and N_2O_3, *J. Photochem.*, *8*, 193–203, 1978.

Stuhl, F., and H. Niki, Flash photochemical study of the reaction OH + NO + M using resonance fluorescent detection of OH, *J. Chem. Phys.*, *57*(9), 3677–3679, 1972.

Stutz, J., Messung der Konzentration troposphärischer Spurenstoffe mittels Differentieller Optischer Absorptionspektroskopie: Eine neue Gerneration von Geräten und Algorithmen, Ph.D. thesis, Univ. Heidelberg, Heidelberg, Germany, 1996.

Stutz, J., and U. Platt, Problems in using diode arrays for open path DOAS measurements of atmospheric species, paper presented at Symposium Optical Methods in the Atmospheric Chemistry, Eur. Opt. Soc., SPIE-Int. Soc. for Opt. Eng., Berlin, 1992.

Stutz, J., and U. Platt, Numerical analysis and estimation of the statistical error of differential optical absorption spectroscopy measurements with least squaress methods, *Appl. Opt.*, *35*(30), 6041–6053, 1996.

Stutz, J., and U. Platt, Improving long-path differential optical absorption spectroscopy with a quartz-fiber mode mixer, *Appl. Opt.*, *36*(6), 1105–1115, 1997.

Stutz, J., E. S. Kim, U. Platt, P. Bruno, C. Perrino, and A. Febo, UV-visible absorption cross section of nitrous acid, *J. Geophys. Res.*, *105*, 14,585–14,592, 2000.

Stutz, J., B. Alicke, and A. Neftel, Nitrous acid formation in the urban atmosphere: Gradient measurements of N_2O and HONO over grass in Milan, Italy, *J. Geophys. Res*, *107*, 10.1029/2001JD000390, in press, 2002.

Svensson, R., E. Ljungström, and O. Lindqvist, Kinetics of the reaction between nitrogen dioxide and water vapour, *Atmos. Environ.*, *21*, 1529–1539, 1987.

Vandaele, A. C., P. C. Simon, J. M. Guilmot, M. Carleer, and R. Colin, SO_2 absorption cross section measurement in the UV using a Fourier transform spectrometer, *J. Geophys. Res.*, *99*, 25,599–25,605, 1994.

Winer, A. M., and H. W. Biermann, Long path length differential optical absorption spectroscopy (DOAS) measurements of gaseous HONO, NO_2 and HCHO in the California South Coast Air Basin, *Res. Chem. Interm.*, *20*(3–5), 423–445, 1994.

Zabarnick, S., Kinetics of the reaction OH + NO + M –> HONO + M as a function of temperature and pressure in the presence of argon, SF_6, and N_2 bath gas, *Chem. Phys.*, *171*(1–2), 265–273, 1993.

B. Alicke and J. Stutz, Department of Atmospheric Sciences, 7172 Math Sciences, Box 951565, UCLA, Los Angeles, CA 90095-1565, USA. (jochen@atmos.ucla.edu)

U. Platt, Institut für Umweltphysik, INF 229, D-69120 Heidelberg, Germany.

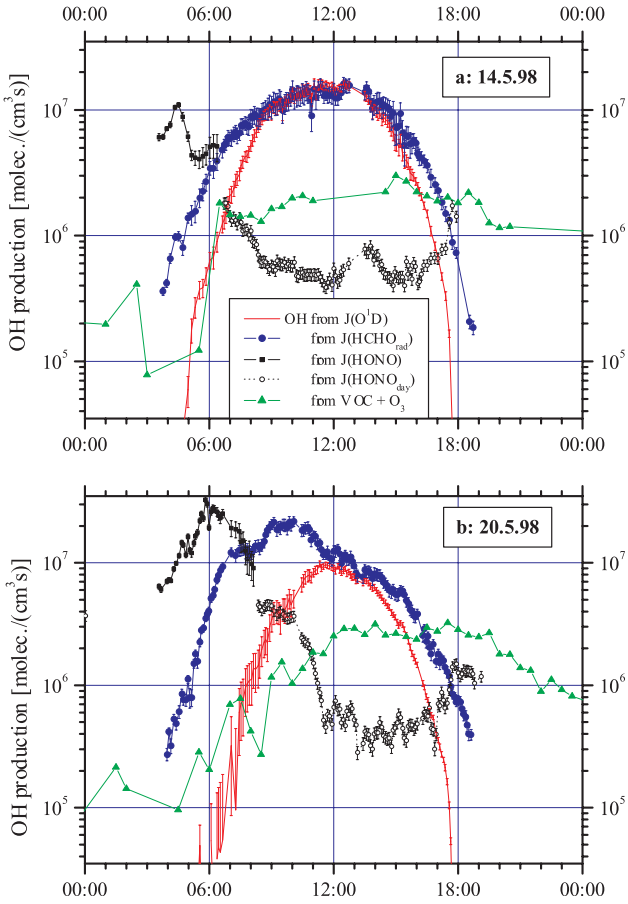

Figure 13. Comparison of four different OH-radical-producing processes for (a) 14 May 1998 and (b) 20 May 1998. The data are plotted on a logarithmic scale for a better overview. The impact of HONO photolysis on the OH formation in the early morning hours can be easily seen. The estimated daytime OH production from HONO (see text) is shown with a dotted line.